Eva Maria Holzer, BSc

Influence of perfect nesting on the spin-density and charge-density waves in the extended Hubbard model

MASTER'S THESIS

to achieve the university degree of

Diplom-Ingenieurin

Master's degree programme: Technical Physics

submitted to

Graz University of Technology

Supervisor

Assoc.Prof. Dipl.-Ing. Dr.techn. Markus Aichhorn

Institute of Theoretical and Computational Physics

Graz, October 2020

'...dass ich erkenne, was die Welt
im Innersten zusammenhält...'
- Goethe, Faust I

Affidavit

I declare that I have authored this thesis independently, that I have not used other than the declared sources/resources, and that I have explicitly indicated all material which has been quoted either literally or by content from the sources used. The text document uploaded to TUGRAZonline is identical to the present master's thesis.

Date	Signature

Abstract

This thesis reviews different approaches to the extended Hubbard Hamiltonian with mean-field and finite-size cluster approximations. The phase diagrams including spin-density and charge-density waves in the one-dimensional, square and honeycomb lattices are investigated. The inclusion of the next-nearest neighbour hopping results in a change of the Fermi surface. As a consequence, the systems do not exhibit perfect nesting any more for the one-dimensional and square lattice. The honeycomb lattice has no perfect nesting in two-dimensions. We highlight the importance of perfect nesting for a finite critical interaction value. The one-dimensional lattice gets further analysed with a combination of mean-field approximation and a cluster extension, which is treated numerically by means of exact diagonalization.

Contents

Acknowledgements

I have received a great deal of support and assistant throughout the writing of this work.

First, I would like to thank my supervisor, Professor Markus Aichhorn, for all his help and advice. Without his insightful comments, suggestions and patience during the finish of my master study, this would have not been possible. I want to thank my colleagues from the Institute of Theoretical and Computational Physics at the University of Technology Graz. Especially, thanks to Dipl. Ing. Markus Richter, for his helpful ideas and answers. Thanks to Dr. Omar Veledar, for his detailed comments and suggestions on the thesis.

Thanks to my parents, for the opportunity of my exchange year and the support throughout my study. I want to thank my brothers and their families, for giving me a place to stay and having an open ear.

And I want to thank my friends. I could not have finished this thesis without the stimulating discussions as well as happy distractions to rest my mind outside of my research.

List of Figures

1 Introduction

The Hubbard model [1] is essential in the theoretical condensed matter physics. Especially the understanding of strongly correlated electrons is an important goal, as discussed in [2]. A good example of this correlation effects is magnetism, where electrons reduce the energy cost of the Coulomb interaction by ordering.

Initially the model was applied to the behaviour of transition-metal monoxides in the early 1960's [3], but it has a much broader application range. It gives insight into insulating, magnetic and novel superconducting effects in a solid.

The objective of this work is to show different quantum phase transitions through different routes. The extended Hubbard Hamiltonian for the one-dimensional, square and honeycomb lattice is discussed with and without next-nearest neighbour hopping. The inclusion of the next-nearest neighbour hopping results in a change of the Fermi surface. This change destroys the so called perfect nesting property of the systems, which has an important effect on the critical interaction values of the phase transitions.

The Hubbard Hamiltonian has been studied in the whole area of analytic techniques common in the condensed matter physics community. In this work the static mean-field approach is used. In the last chapter it is extended to include short-range fluctuations in finite size clusters, which are treated by the numerical method of exact diagonalization.

2 Models and Methods

The first part of this chapter is based on literature [4]. The non-relativistic time-independent full Schrödinger equation can be written as

$$\hat{H} |\phi\rangle = \epsilon |\phi\rangle \tag{2.1}$$

where $\hat{H}$ is the Hamiltonian operator that describes a system of nuclei and electrons. $|\phi\rangle$ are the eigenstates and ϵ are the eigenenergies of the system. For N electrons and M nuclei the Hamiltonian is

$$\begin{aligned} \hat{H} = -\sum_{i=1}^{N} \frac{1}{2}\nabla_i^2 - \sum_{A=1}^{M} \frac{1}{2M_A}\nabla_A^2 - \sum_{i=1}^{N}\sum_{A=1}^{M} \frac{Z_A}{r_{iA}} \\ + \sum_{i=1}^{N}\sum_{j>i}^{N} \frac{1}{r_{ij}} + \sum_{A=1}^{M}\sum_{B>A}^{M} \frac{Z_A Z_B}{R_{AB}}. \end{aligned} \tag{2.2}$$

Z_A is the atomic number of the nucleus A and M_A is the ratio of the mass of the nucleus A to the mass of an electron. The kinetic energy of the electrons is described by the first term in equation 2.2 and the second term describes the kinetic energy of the nuclei. The coulomb interaction between electrons and nuclei is represented in the third term. The fourth term is the repulsion between electrons and the fifth term is the repulsion between nuclei.

The Schrödinger equation 2.1 is mostly solved with the Born-Oppenheimer approximation. This approximation considers that nuclei are much heavier than electrons. The nuclei move more slowly than the electrons. This leads to the approximation that the electrons in a molecule or solid move in the field of fixed nuclei. The kinetic energy of the nuclei can be neglected without movement and the second term of equation 2.2 vanishes. The repulsion between nuclei, last term in equation 2.2, is a constant in the Born-Oppenheimer approximation. The addition of any constant to an operator

only adds to its eigenvalues and has no effect on its eigenfunctions. The remaining three terms of equation 2.2 are called the electronic Hamiltonian. It describes the motion of N electrons in the field of M point charges and can be written as

$$\hat{H}_{elec} = -\sum_{i=1}^{N} \frac{1}{2}\nabla_i^2 - \sum_{i=1}^{N}\sum_{A=1}^{M} \frac{Z_A}{r_{iA}} + \sum_{i=1}^{N}\sum_{j>i}^{N} \frac{1}{r_{ij}}, \tag{2.3}$$

where the first term is the electron kinetic energy, the second term is the lattice potential and the third term is the interaction of the electrons. The electron-electron interaction in the electronic Hamiltonian leaves a complex many-body problem and needs further adaptation. One available way to solve the equation is the free-electron approximation. It simply neglects the interaction part, which is sometimes reasonable for good metals, but fails for insulators and semiconductors. The Hubbard model is one way to further simplify the interaction term and find approximations to make it tractable.

2.1 Second Quantization

The Hamiltonian described in equation 2.3 depends only on the spatial coordinates of the electrons. For the complete description of an electron also the spin of the electron has to be taken into account. In the context of the nonrelativistic theory there are two spin eigenfunctions, spin up and spin down. The Hamiltonian does not reference to the spin and simply making the wavefunction dependent on the spin is not enough. The requirement for the electronic wavefunction is that the function must be antisymmetric with respect to the interchange of any two electrons' coordinates. The coordinate is both, space and spin. This requirement is called the antisymmetry principle and is a general statement of the Pauli exclusion principle. The exact wavefunction has to satisfy the Schrödinger equation and must be antisymmetric in the spatial and the spin coordinate.

The antisymmetry is easily established by the usage of Slater determinants. For an N-electron system the generalised determinant is

$$\left|\phi^N\right\rangle = \frac{1}{\sqrt{N!}} \begin{vmatrix} \left|\phi_1^{(1)}\right\rangle & \left|\phi_1^{(2)}\right\rangle & \cdots & \left|\phi_1^{(N)}\right\rangle \\ \left|\phi_2^{(1)}\right\rangle & \left|\phi_2^{(2)}\right\rangle & \cdots & \left|\phi_2^{(N)}\right\rangle \\ \vdots & \vdots & & \vdots \\ \left|\phi_N^{(1)}\right\rangle & \left|\phi_N^{(2)}\right\rangle & \cdots & \left|\phi_N^{(N)}\right\rangle \end{vmatrix} \tag{2.4}$$

with the normalization factor $\frac{1}{\sqrt{N!}}$. The Slater determinant has N fermions occupying N states without specifying which electron is in which state. Interchanging the coordinates of two fermions corresponds to interchanging two rows of the Slater determinant. This changes the sign of the determinant. Therefore the requirement of the antisymmetry principle is fulfilled. Two fermions occupying the same state leads to two equal columns of the determinant. This would make the determinant equal to zero and no more than one fermion can occupy one state. The Pauli exclusion principle is fulfilled.

The short hand notation, of the Slater determinant, shows only the diagonal elements of it

$$\left|\phi^N\right\rangle = \left|\phi_1\phi_2...\phi_N\right\rangle, \tag{2.5}$$

which includes the normalization constant implicitly.

A convenient description for many-body problems is the second quantization. It uses certain algebraic properties of operators to realize the antisymmetry property of the wave function.

The properties of the determinants are shifted to the algebraic properties of operators. One of this operators is the so called creation operator $c_{j\sigma}^\dagger$. The definition of $c_{j\sigma}^\dagger$ is

$$c_{j\sigma}^\dagger \left|n_{1\sigma}...n_{j\sigma}...\right\rangle = \sqrt{n_{j\sigma}+1}\left|n_{1\sigma}...\ (n_{j\sigma}+1)\ ...\right\rangle. \tag{2.6}$$

It creates a fermion of spin σ on site j. $n_{j\sigma}$ is the occupation number.

The adjoint of the creation operator is the annihilation operator $c_{i\sigma'}$. In analogy to equation 2.6 $c_{i\sigma'}$ is defined as

$$c_{i\sigma'} \left| n_{1\sigma'} ... n_{i\sigma'} ... \right\rangle = \sqrt{n_{i\sigma'}} \left| n_{1\sigma'} ... \left(n_{i\sigma'} - 1 \right) ... \right\rangle . \tag{2.7}$$

It annihilates or destroys a fermion of spin σ' on site i. The direct relation between the two operators is $(c^{\dagger}_{j\sigma})^{\dagger} = c_{j\sigma}$. Besides that, there are three important anticommutation relations between a creation and an annihilation operator. The first one is

$$\{c_{i\sigma}, c^{\dagger}_{j\sigma'}\} = c_{i\sigma}, c^{\dagger}_{j\sigma'} + c^{\dagger}_{j\sigma'}, c_{i\sigma} = \delta_{i,j}\delta_{\sigma,\sigma'}. \tag{2.8}$$

This expression shows that the interchange of a creation and an annihilation operator, which refer to same spin and spatial coordinates, is different to the interchange, if they have the same coordinates. The other two anticommutaion relations are

$$\{c^{\dagger}_{i\sigma}, c^{\dagger}_{j\sigma'}\} = 0 \tag{2.9}$$

$$\{c_{i\sigma}, c_{j\sigma'}\} = 0. \tag{2.10}$$

These relations imply that it is not possible to create or destroy two fermions with the same coordinates.

A Slater determinant represented in the second quantization is

$$c^{\dagger}_{1\sigma} c^{\dagger}_{2\sigma} \left| 0 \right\rangle = \left| \phi_1 \phi_2 \right\rangle , \tag{2.11}$$

with the vacuum state $|0\rangle$.

The occupation number is defined as $n_{j\sigma} = c^{\dagger}_{j\sigma} c_{j\sigma}$. For fermions it can be zero or one, the site can be occupied or empty. The occupation number representation of the basis state is

$$\left| n \right\rangle = \left| n_{1,\sigma}, n_{2,\sigma}, n_{3,\sigma}, ... \right\rangle . \tag{2.12}$$

The number operator is defined as the sum over the occupation numbers

$$N = \sum_{i\sigma} n_{i\sigma} = \sum_{i\sigma} c^{\dagger}_{i\sigma} c_{i\sigma}. \tag{2.13}$$

The operator counts the number of the particles in the system. It can be written as

$$N\,|n\rangle = n\,|n\rangle\,, \tag{2.14}$$

where $|n\rangle$ is the eigenvector and n is the eigenvalue.

2.1.1 Bloch's theorem

Bloch's theorem states that the eigenstates $\phi_{\mathbf{k}}$ of a one-electron Hamiltonian can be chosen to be a plain wave multiplied with a function that has the periodicity of the Bravaise lattice. It has the form

$$\phi_{\mathbf{k}}(\mathbf{r}+\mathbf{T}) = e^{2\pi i \mathbf{r}\cdot\mathbf{T}}\phi_{\mathbf{k}}(\mathbf{r}), \tag{2.15}$$

where the vector $\mathbf{T}$ is the lattice vector between the unit cells. The Bloch theorem gives for each $\mathbf{k}$-point in the Brillouin zone a Bloch basis orbital

$$\phi(\mathbf{k}) = \frac{1}{\sqrt{N}}\sum_{\mathbf{T}} e^{2\pi i \mathbf{r}\cdot\mathbf{T}}\phi(\mathbf{T}), \tag{2.16}$$

with the sum over $\mathbf{T}$ for every unit cell in the lattice.

2.2 Strongly correlated Electrons

In materials with strongly correlated electrons, the metallic character of the material is suppressed in favour of an insulating state. This is discussed in detail in literature [5]. The following section shortly reviews some important features of strongly correlated electrons.

An important aspect of electron correlations is the partial suppression of electronic charge fluctuations on an atomic site. Those are called inter-atomic correlations because the fluctuations are caused by the overlap of wavefunctions from different atoms. The electronic delocalization causes a kinetic energy gain which favours the inter-atomic correlations.

For electrons on the same atom intra-atomic correlations must be considered. Hund's rules and in-out correlations are responsible for the optimization

of the on-site Coulomb repulsions of those electrons. In-out correlations describe the behaviour of a system, when one electron sits close to the nucleus and the other electrons consequently stay further away from it. Hund's rules are regulating the optimal angular distribution of the atom segments to minimize their repulsions. The radial distribution of the electrons is managed by the in-out correlations.

Intra-atomic correlations can still be strong with weak inter-atomic correlations. Intra-atomic correlations are important for 4f electrons and transition-metal ions. Transition metals are in the middle between the limits of uncorrelated and strongly correlated electrons.

Charge order appearance is an additional aspect of strongly correlated electrons. There is a minimization of the repulsive energy between electrons for a charge order state. This happens at the expense of the kinetic energy. In comparison to the homogeneous systems, the inhomogeneous systems have a larger probability of charge ordering. An inhomogeneous system is for example a lattice. The delocalization in inhomogeneous electron systems reduces the kinetic energy gain compared to homogeneous electron systems.

Charge order does not occur in the standard Hubbard Model. It needs the presence of inter-site interaction. The extended Hubbard model gives the mandatory surroundings to study the desired orders, as shown in the following sections.

2.3 The extended Hubbard Hamiltonian

The extended Hubbard model is a very simple and yet successful model for the description of electron interactions in solids. It takes inter-electronic interactions as well as their kinetic energy into account. The nuclear positions are considered fixed and there is a lattice of atoms or sites on which the fermions are able to move. The Hubbard model simplifies the atoms in a solid to a collection of sites, each with a single orbital. If a solid has just one energy band at the Fermi surface, it has only one relevant orbital and the Hubbard Hamiltonian is a good picture for it.

There are four different possible configurations for the sites of the Hubbard Hamiltonian. It can be empty, a single down fermion, a single up fermion or it is occupied by a pair of up and down fermions. Electrons in a solid, which are able to move around, interact over a screened Coulomb interaction. The biggest interactions is for electrons on the same site, as it is discussed in [3]. The on-site interactions are defined by a term which is zero for an empty or single occupied site and has the value U for an double occupied site. The Coulomb interaction between fermions on close-by sites is given by the value V. The kinetic energy is explained by an expression which destroys a fermion on one site and creates it on a another site. The hopping between the sites is governed by the energy scale t. It is determined by the overlap of two wavefunctions on the atoms, which die off exponentially. For the model in this work only a hopping between the nearest neighbours (NN) and the next nearest neighbours (NNN) is included.

The extended Hubbard Hamiltonian can be written as

$$H = -\sum_{ij,\sigma} t_{i,j}(c^{\dagger}_{i\sigma}c_{j\sigma} + h.c.) + \frac{U}{2}\sum_{i\sigma} n_{i\sigma}n_{i\sigma'} + V\sum_{i>j} n_i n_j - \mu\sum_i n_i. \tag{2.17}$$

The first term in equation 2.17 is the hopping term. It describes the kinetic energy. On its own it is the single particle solution of the Hubbard Model for non-interaction fermions. $c_i^{\dagger}$ is the creation operator, see equation 2.6, and c_j is the annihilation operator, see equation 2.7.

In general the coefficients t_{ij} characterize the single particle matrix elements defined by the overlap integral derived in [6]

$$t_{ij} = -\int d\mathbf{r}\Phi_i^*(\mathbf{r})(-\frac{\hbar^2\nabla^2}{2m} + V(\mathbf{r}))\Phi_j(\mathbf{r}-\mathbf{R}), \tag{2.18}$$

where $\mathbf{R} = \mathbf{r_i} - \mathbf{r_j}$ describes the hopping distance, $V(\mathbf{r})$ represents the periodic crystal potential energy and $-\frac{\hbar^2\nabla^2}{2m}$ is the kinetic energy of the one particle term. The hopping amplitude does not depend on the spin σ, but it is sensitive to the band structure. The restriction of the hopping term t is

$$t_{ij} = \begin{cases} t & \text{if } i,j \text{ are nearest neighbour,} \\ -t' & \text{if } i,j \text{ are next nearest neighbours,} \\ 0 & \text{otherwise.} \end{cases} \tag{2.19}$$

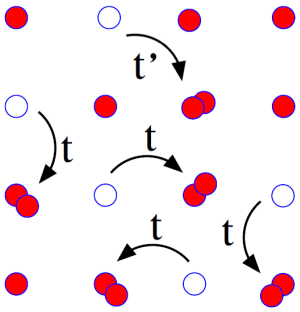

Figure 2.1: Hopping on square lattice, representing the kinetic energy of the Hubbard Hamiltonian (altered from [3]).

In the following equations, the NN hopping constant is $t = 1$ and the NNN hopping constant t' alters in the region $0.0 < t'/t < 1.0$. The neighbouring sites have the largest overlap and therefore a greater probability of hopping. Figure 2.1 depicts a schematic representation of the two different ways the hopping can occur for a square lattice.

The t-Hamiltonian is mathematically identical to the "tight-binding" approach to electron bands, but it has a different intent. Every independent-electron model will yield similar qualitative behaviour, this model adopts the simplest one, similar to the free-electron model in the theory of metals.

The second term in the Hubbard Hamiltonian equation 2.17 describes the on-site interaction. The term adds the energy U at doubly occupied sites each of which being occupied by one the spin up and one spin down fermion. If the fermions belong to two separate sites they do not feel this repulsion. On its own, the on-site term describes a purely atomic picture. The on-site Coulomb repulsion is

$$U = \frac{e^2}{4\pi\epsilon_0} \int d\mathbf{r} d\mathbf{r}' |\Phi_{i\sigma}(\mathbf{r})|^2 \frac{1}{|\mathbf{r} - \mathbf{r}'|} |\Phi_{i\tilde{\sigma}}(\mathbf{r}')|^2. \tag{2.20}$$

The on-site term does not depend on the site label i, if the system is homogeneous.

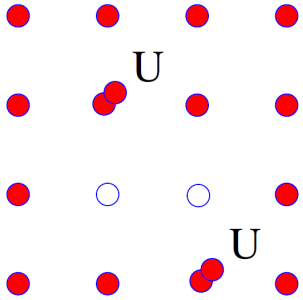

Figure 2.2: On-site interaction on a square lattice (altered from [3]).

The third term in the Hubbard Hamiltonian equation 2.17 is the interaction term between nearest neighbour fermions. It includes the inter-site electron-electron interaction V. The inter-site Coulomb repulsion is

$$V = \frac{e^2}{4\pi\epsilon_0} \int d\mathbf{r} d\mathbf{r}' |\Phi_{i\sigma}(\mathbf{r})|^2 \frac{1}{|\mathbf{r} - \mathbf{r}'|} \left|\Phi_{j\sigma'}(\mathbf{r}')\right|^2. \tag{2.21}$$

This term depends on the spin σ and on the site labels i and j. In this model, we only take into account the terms, where i and j are nearest neighbours. Figure 2.3 shows an interaction between nearest neighbours.

The interaction parameters U and V are repulsive $U, V > 0$ and $U > V$ if they arise from Coulomb interactions. There are additional effects from e.g. electron-photon interactions that can broaden this range of the parameters, but those are not considered for these calculations. The interaction parameters U and V are expressed in the energy units of t.

The last term in the extended Hubbard Hamiltonian equation 2.17 is a chemical potential μ which controls the filling. The Hubbard Hamiltonian has an implied parameter, the band filling ρ. The band filling is defined as

$$\rho = \frac{N_e}{N_c} \tag{2.22}$$

with the number of electrons N_e and the total number of sites N_c in the system. If there is one fermion per site the situation is called half-filling, the lattice contains half as many fermions as the maximum number, which is

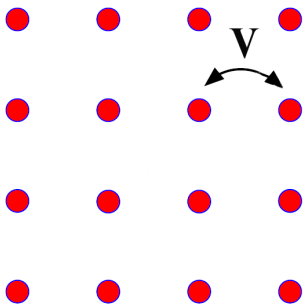

Figure 2.3: Inter-site interaction on a square lattice (altered from [3]).

two per site. This work only deals with half filling and the band filling is always $\rho = 1$.

2.3.1 Particle-hole Symmetry

The extended Hubbard Hamiltonian has a particle-hole symmetry without the next nearest neighbour hopping ($t'/t = 0$). For the description of the particle-hole symmetry, it is important to define a bipartite lattice. A bipartite lattice is a lattice where the set of sites are divided into two sublattices, A and B. The sublattices are ordered in a way that the site A only has B neighbours and vice versa. The one dimensional, square and honeycomb lattices are bipartite. A triangular lattice, for example, is not bipartite. The bipartite lattice supports the antiferromagnetic order. The spin up electrons can occupy a separated sublattice from the spin down electrons. In a triangular lattice the antiferromagnetic order is frustrated.

The particle-hole transformation is introduced with the definition of new operators. Those operators exchange the role of creation and destruction

$$d_{i\sigma}^{\dagger} = (-1)^i c_{i\sigma}. \tag{2.23}$$

The sign factor $(-1)^i$ becomes -1 on sublattice A and +1 at sublattice B. The particle-hole transformation immediately leads to

$$d_{i\sigma}^{\dagger} d_{i\sigma} = 1 - c_{i\sigma}^{\dagger} c_{i\sigma}. \tag{2.24}$$

The eigenstates of the number operators are interchanged. In other words, the occupations exchange. The kinetic energy of the Hubbard Hamiltonian between neighbouring sites under the particle-hole transformation can be seen as

$$c^{\dagger}_{i\sigma}c_{j\sigma} \rightarrow -d_{i\sigma}d^{\dagger}_{j\sigma} = d^{\dagger}_{j\sigma}d_{i\sigma} \tag{2.25}$$

where one minus sign arises from the anticommutation of the operators and the second minus sign arises from the bipartite nature of the lattice. The minus sign annihilate each other and kinetic energy is particle-hole symmetric

$$t \rightarrow t. \tag{2.26}$$

The Coulomb interaction terms of the Hubbard Hamiltonian can be rewritten as

$$U(n_{i\uparrow} - \frac{1}{2})(n_{i\downarrow} - \frac{1}{2}) + V(n_i - 1)(n_j - 1) \tag{2.27}$$

which is unchanged under particle-hole transformation at $\mu = 0$. This new form of the Coulomb interaction gives an additive constant to the energy. With the knowledge of the equations 2.26 and 2.27 the Hamiltonian, under the particle-hole transformation, is

$$H = -t \sum_{\langle i,j\rangle\sigma} \left(c^{\dagger}_{i\sigma}c_{j\sigma} + c^{\dagger}_{j\sigma}c_{i\sigma}\right) + U\sum_i n_{i\uparrow}n_{i\downarrow} + V\sum_{ij} n_i n_j - \mu\sum_i n_i. \tag{2.28}$$

Equation 2.28 is equivalent to the original Hubbard Hamiltonian, with the exception of the chemical potential and the additive energy constant. The chemical potential has a shift of

$$\mu = \frac{U}{2} + zV. \tag{2.29}$$

This shift ensures half filling, $\rho = 1$, under the particle-hole symmetry. The symmetry shows, that the whole phase diagram of the bipartite lattice is symmetric about half-filling. This means that there are as many excited holes as there are excited electrons. For a temperature shift there is no shift in the Fermi level and there are no thermoelectric effects. This is only valid for nearest neighbour hopping.

If next nearest neighbour hopping t' is included, $t'/t \neq 0$, the particle-hole symmetry breaks and the properties of the Hubbard Hamiltonian are not the same above and below half-filling. The kinetic energy between the next nearest neighbouring sites under the particle-hole transformation looks like

$$c^\dagger_{i\sigma} c_{j\sigma} \rightarrow d_{i\sigma} d^\dagger_{j\sigma} = -d^\dagger_{j\sigma} d_{i\sigma} \tag{2.30}$$

where the minus sign doesn't vanish, because i and j are second neighbours and the kinetic energy for the next nearest neighbour hopping is not particle-hole symmetric

$$t' \rightarrow -t'. \tag{2.31}$$

It shows that electron- and hole-doped solids have different properties and in realistic bands there is usually no particle-hole symmetry as well as in the free electron dispersion.

Perfect Nesting

The Fermi Surface of the Hubbard Hamiltonian is calculated from the energy dispersion relation and separates filled and empty states at the absence of interactions. Perfect nesting describes a reciprocal lattice vector that maps an entire section of the Fermi surface onto another one. The square lattice has this unique feature at half filling, as described in [7]. The reciprocal vector in the square lattice model is for example $(-\pi/a, \pi/a)$. The nesting occurs due to the fact, that it is a bipartite lattice and the kinetic energy only connects one sublattice to another. In other words, there is no perfect nesting if next nearest neighbour hopping is included. Figure 2.4 shows the perfect nesting of a square lattice at the absence of next nearest neighbour hopping and on the right side the loss of perfect nesting with the hopping constant $t' = 0.2$ with different chemical potential. Lowering the chemical potential corresponds to a hole doping.

The one dimensional lattice has of course also the feature of perfect nesting. The reciprocal lattice vector that maps the one dimensional Fermi surface onto another is $(\pi/2a)$

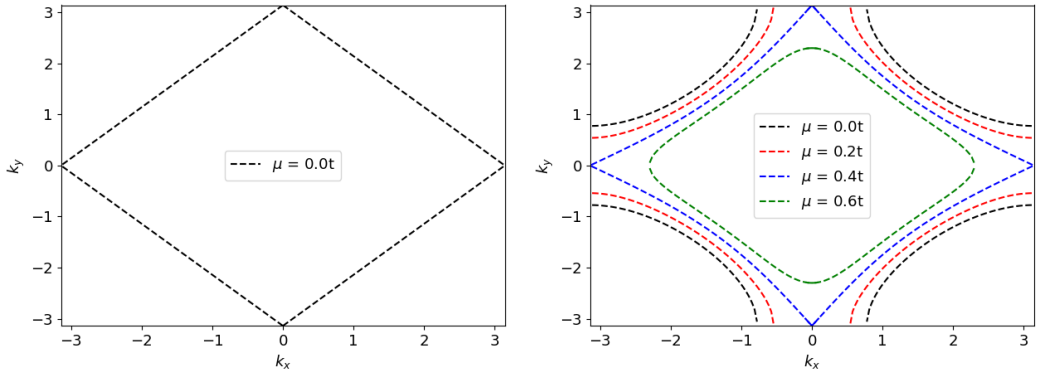

Figure 2.4: Fermi surface for the square lattice shows the perfect nesting for $t'/t = 0.0$ on the left and the loss of perfect nesting for $t'/t = 0.2$ on the right at different chemical potential μ.

2.4 Phases and Phase transitions

A phase transition is happening when we see a change in the properties of a system at a certain point in phase space. It can precisely be defined through an order parameter, which is zero on one side of the transition, and non-zero on the other side.

If there is an absence of the interactions U and V, the ground state is that of uncorrelated electrons and has the form of a Slater determinant. A lattice site can have four different configurations, as mentioned before. Each configuration has relative weights dependent on the form of the Slater determinant. At half filling and with $t'/t = 0$ all four states have the same probability. There is no preferred ordering. The kinetic energy delocalizes the electrons by putting individual electrons in Bloch states. This t-model limit, also known as band limit, always describes a metal.

With increasing on-site interaction term U there is an additional energy per site and the weight of the doubly occupied sites must reduce. The hopping term t and interaction term U compete with each other, as discussed in [8]. In the limit $U \gg t$ the doubly occupied configurations of a single site in the Hamiltonian costs a large energy. That means that at half filling the ground state charge distribution adjusts itself to avoid doubly occupied states for

large U and there is a spin-density wave (SDW). The charge fluctuations around the occupation number $n_{j\sigma} = 1$ configuration are very expensive. The costs of charge fluctuations increase with U. There is a critical value U_{MIT} of the order of band width beyond the material is an insulator. The band width W is defined as

$$W = 2zt, \tag{2.32}$$

with the coordination number z and without the second neighbour hopping $t'/t = 0$. The charge fluctuations are frozen and this first order phase transition is known as Mott metal-insulator transition. An additional feature of the increasing U is that the antiferromagnetic correlations between neighbouring sites become more important. A reduction of doubly occupied sites results in antiferromagnetic correlations. In case of half filling a spin-density wave ground state reduces to an antiferromagnetic state.

The energy difference in insulators and semiconductors between the bottom of the conduction band and the top of the valence band is called band gap. In the mean-field approximation, which is explained in the following chapter, the band gap can be described with the gap equation. The gap equation for the antiferromagnetic ordering, shown in [7], is

$$\begin{aligned} 1 &= \frac{U}{N} \sum_{\mathbf{k}} \frac{1}{\sqrt{E_{\mathbf{k}}^2 + G^2}} \\ &= U \int_{\mu}^{0} d\epsilon \frac{\rho(\epsilon)}{\sqrt{\epsilon^2 + G^2}} \end{aligned} \tag{2.33}$$

with the size of the gap $G \sim Um$ and the density of states $\rho(\epsilon)$, see equation 2.34. If there is perfect nesting, there is a special solution with $G \neq 0$ for arbitrarily small U. If there is a $t'/t \neq 0$ there is $G = 0$ for small U expected, because the perfect nesting is destroyed.

The one-band models prefer the formation of an antiferromagnetic ordering [8], but under certain conditions there is the possibility of ferromagnetic states [9].

With the inclusion of the inter-site interactions V the study of inhomogeneous phases, such as charge-density waves (CDW), is possible. The phase has broken discrete symmetry which is characterized by alternating doubly occupied sites and empty sites. It exhibits long-range order.

The spin fluctuations are dominant when the electron-electron interaction is short ranged, there are spin-density waves. The standard Hubbard model is an example for this phenomena. With an increasing range of the electron-electron interactions, the charge fluctuations get more intense and there can be charge-density waves. In some cases coexistence of both fluctuations is possible and spin-density waves as well as charge-density waves can be found. Figure 2.5 shows the behaviour of the electrons for spin-density and charge-density waves. A good guideline for charge and spin-density waves is the rule for positive interaction strengths given in [10]. If $U < zV$, the ground state is a charge-density wave and if $U > zV$, the ground state is a spin-density wave.

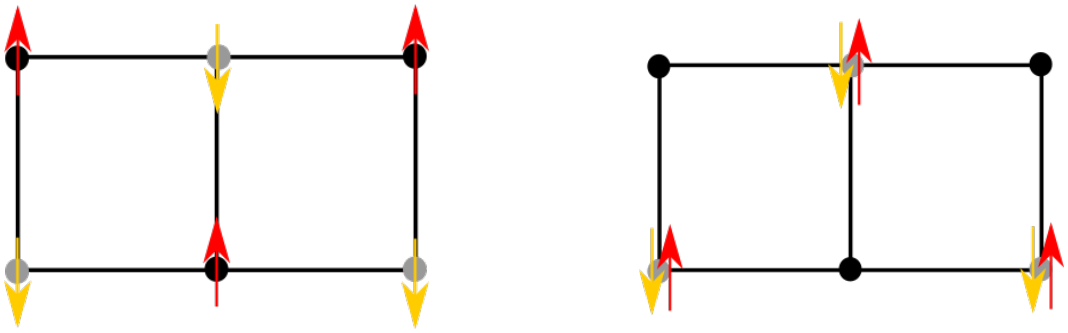

Figure 2.5: Spin-density wave on the left with $U/t \gg 1$, $V = 0$ and charge-density wave on the right with $U = 0$, $V/t \gg 1$ as preferred ordering.

The density of states $\rho(\epsilon)$ per unit cell is defined as

$$\rho(\epsilon) = \frac{1}{N} \sum_{ki\sigma} \delta(\epsilon - \epsilon_{i\sigma}(\mathbf{k})). \tag{2.34}$$

The chemical potential μ is given by the implicit equation

$$\int_{-\infty}^{\infty} d\epsilon \rho(\epsilon) \frac{1}{e^{\beta(\epsilon-\mu)}} = N_e \tag{2.35}$$

where $\beta = 1/k_B T$ is the Boltzmann factor and N_e is the total number of electrons per unit cell. The average number of particles per site at temperature T are given by

$$\langle n_{i\sigma} \rangle = \frac{1}{N_k} \sum_{\mathbf{k},m} |u_{m\mathbf{k}}|^2 \frac{1}{e^{\beta(\epsilon(\mathbf{k})-\mu))}}. \tag{2.36}$$

The variable $u_{m\mathbf{k}}$ represents the occupied eigenstates in the system.

In this work, we study the ground-state phase diagram of the extended Hubbard model. This means, that we do calculations at zero temperature $T = 0$, and the only state that contributes to the expectation value is the ground state.

2.4.1 Quantum Phase transitions

A phase transition can occur through different routes. In the case that the transition is not driven by temperature and happens at zero temperature, it is called quantum phase transition. Different routes for quantum phase transitions were investigated in [11].In the extended Hubbard Hamiltonian they can be controlled by the following points

- *Bandwidth control*
  The relative strength of the electron interaction and the relative transfer t'/t in the Hamiltonian are controlling the bandwidth.
- *Band filling control*
  The band model is half filled for the following calculations $\rho = 1$.
- *Lattice structure control*
  In the Hubbard Hamiltonian the lattice structure information is in the hopping constant t_{ij}.

This control parameters can be realized by doping, pressure and chemical composition and magnetic fields for example. In case of perfect nesting the phase transition is happening at an interaction value of zero [12]. The phase transition is happening at non-zero interaction with the destruction of the perfect nesting.

3 Mean-Field Approximation

One important method to deal with many body systems is the mean-field theory. It is a method for systems with interactions, where the full system is replaced by an effective one-body problem with a chosen external field. The interaction of all particles to an arbitrary particle is replaced by this external field which has to be determined self-consistently. The mean-field approximation is not sufficient for the description of electronic correlations, because the fluctuations are not respected. However, it can be applied to many different physical systems to study phenomena such as the phase transition. It ignores quantum fluctuations and therefore is less accurate in lower spatial dimensions. Mean-field ignores both spatial and temporal fluctuations.

The fluctuations around the mean density are defined as

$$\delta n_{i\sigma} = n_{i\sigma} - \langle n_{i\sigma} \rangle, \tag{3.1}$$

where the fluctuations δn are the difference between the exact number operator $n_{i\sigma}$ and the mean occupation number $\langle n_{i\sigma} \rangle$.

Using definition 3.1, we can rewrite the on-site interaction part as

$$\begin{aligned} \sum_i n_{i\uparrow} n_{i\downarrow} &= \sum_i [\delta n_{i\uparrow} + \langle n_{i\uparrow} \rangle][\delta n_{i\downarrow} + \langle n_{i\downarrow} \rangle] \\ &= \sum_i [\delta n_{i\uparrow} \delta n_{i\downarrow} + \delta n_{i\downarrow} \langle n_{i\uparrow} \rangle + \delta n_{i\uparrow} \langle n_{i\downarrow} \rangle + \langle n_{i\uparrow} \rangle \langle n_{i\downarrow} \rangle]. \end{aligned} \tag{3.2}$$

The fluctuations $\delta n_{i\uparrow}$ and $\delta n_{i\downarrow}$ are supposed to be so small that the quadratic term in the second line is negligible. The term $\sum_i n_{i\uparrow} n_{i\downarrow}$ becomes finally in

the mean-field approximation

$$\begin{aligned}\sum_i n_{i\uparrow}n_{i\downarrow} &\approx \sum_i[\delta n_{i\downarrow}\langle n_{i\uparrow}\rangle + \delta n_{i\uparrow}\langle n_{i\downarrow}\rangle + \langle n_{i\uparrow}\rangle\langle n_{i\downarrow}\rangle] \\ &= \sum_i[(n_{i\downarrow} - \langle n_{i\downarrow}\rangle)\langle n_{i\uparrow}\rangle + (n_{i\uparrow} - \langle n_{i\uparrow}\rangle)\langle n_{i\downarrow}\rangle + \langle n_{i\uparrow}\rangle\langle n_{i\downarrow}\rangle] \\ &= \sum_i[n_{i\downarrow}\langle n_{i\uparrow}\rangle + n_{i\uparrow}\langle n_{i\downarrow}\rangle - \langle n_{i\uparrow}\rangle\langle n_{i\downarrow}\rangle]\end{aligned} \tag{3.3}$$

The on-site term of the extended Hubbard Hamiltonian shown in equation 2.17 becomes therefore

$$H_U^{MF} = U\sum_i[n_{i\downarrow}\langle n_{i\uparrow}\rangle + n_{i\uparrow}\langle n_{i\downarrow}\rangle] - U\sum_i\langle n_{i\uparrow}\rangle\langle n_{i\downarrow}\rangle = H_U + H_{U0} \tag{3.4}$$

where H_{U0} is a constant for given magnetic configuration and number of particles. It only depends on the average density and does not depend on creation or annihilation operators.

The inter-site interaction term of the extended Hubbard Hamiltonian 2.17 under the mean-field approximation becomes

$$H_V^{MF} = zV\sum_{i>j}[n_i\langle n_j\rangle + n_j\langle n_i\rangle] - zV\sum_{i>j}\langle n_i\rangle\langle n_j\rangle = H_V + H_{V0} \tag{3.5}$$

where H_{V0} is only dependent on the average density as explained above and z is the coordination number. The occupation number operators are $n_i = n_{i\uparrow} + n_{i\downarrow}$ and $n_j = n_{j\uparrow} + n_{j\downarrow}$. The densities of those occupation number operators are $\langle n_i\rangle = \langle n_{i\uparrow}\rangle + \langle n_{i\downarrow}\rangle$ and $\langle n_j\rangle = \langle n_{j\uparrow}\rangle + \langle n_{j\downarrow}\rangle$.

The constant energy of the Coulomb interactions is

$$H_0 = H_{U0} + H_{V0} = -U\sum_i\langle n_{i\uparrow}\rangle\langle n_{i\downarrow}\rangle - zV\sum_{i>j}\langle n_i\rangle\langle n_j\rangle. \tag{3.6}$$

The hopping part of the extended Hubbard Hamiltonian 2.17 gives the tight-binding band structure. For the nearest neighbour and the next-nearest

neighbour hopping a Fourier transform to the k-space is transformed, following [6]. The Fourier transform of the annihilation and creation operators are described in the equations 5.2 and 5.1. The k-transformed operators are inserted into the extended Hubbard Hamiltonian, and the tight-binding structure is

$$\begin{aligned} H_t &= \frac{1}{N}\sum_{ij}\sum_{\mathbf{k}\mathbf{k}'\sigma} t_{ij}\, e^{-i\mathbf{k}\mathbf{R_i}} c^{\dagger}_{\mathbf{k}\sigma}\, e^{i\mathbf{k}'\mathbf{R_j}} c_{\mathbf{k}'\sigma} \\ &= \frac{1}{N}\sum_{\mathbf{k}\mathbf{k}'\sigma} c^{\dagger}_{\mathbf{k}\sigma} c_{\mathbf{k}'\sigma} \sum_{ij} t_{ij} e^{-i\mathbf{k}\mathbf{R_i}} e^{i\mathbf{k}'\mathbf{R_j}} \\ &= \sum_{\mathbf{k}\mathbf{k}'\sigma} c^{\dagger}_{\mathbf{k}\sigma} c_{\mathbf{k}'\sigma} \sum_{j} t_{\delta_{\mathbf{ij}}} e^{-i\mathbf{k}'\delta_{ij}} \delta(\mathbf{k}-\mathbf{k}') \\ &= \sum_{\mathbf{k}\sigma} g_k c^{\dagger}_{\mathbf{k}\sigma} c_{\mathbf{k}\sigma}, \end{aligned} \tag{3.7}$$

here the term $g_k = \sum_j t_{\delta_{ij}} e^{-i\mathbf{k}\delta_{\mathbf{ij}}}$ is dependent on the lattice and $\boldsymbol{\delta}_{\mathbf{ij}} = \mathbf{R}_j - \mathbf{R}_i$ connects the sites where the hopping occurs. Moreover the definition of the Kronecker delta is $\delta(\mathbf{k}-\mathbf{k}') = \frac{1}{N}\sum_i e^{-i(\mathbf{k}-\mathbf{k}')\mathbf{R_i}}$.

The matrix representation of the hopping Hamiltonian can be written as

$$H_t = \begin{pmatrix} g'_k & g^*_k & 0 & 0 \\ g_k & g'_k & 0 & 0 \\ 0 & 0 & g'_k & g^*_k \\ 0 & 0 & g_k & g'_k \end{pmatrix} \tag{3.8}$$

where the non-diagonal terms correspond to the nearest neighbour hopping and the diagonal terms correspond to the next-nearest neighbour hopping. The basis state of matrix 3.8 is

$$\phi^{\dagger}_{\mathbf{k}} = [c^{\dagger}_{\mathbf{k},a\uparrow}, c^{\dagger}_{\mathbf{k},b\uparrow}, c^{\dagger}_{\mathbf{k},a\downarrow}, c^{\dagger}_{\mathbf{k},b\downarrow}]. \tag{3.9}$$

The lattice is divided into the two sublattices A and B. The introduced indices a and b represent the decoupled sublattices. This basis state results

in an artificial enlargement of the unit cell. The energy bands for the tight binding solution are

$$E_k^{t,t'} = g'_k \pm g_k. \tag{3.10}$$

One can easily see from equation 3.4 that H_U^{MF} is of one-particle type, with terms such as $U\langle n_{i\uparrow}\rangle$ acting as spin-dependent on-site energies. The matrix form of the on-site interaction of the Hamiltonian is

$$H_U = U \begin{pmatrix} \langle n_{a\downarrow}\rangle & 0 & 0 & 0 \\ 0 & \langle n_{b\downarrow}\rangle & 0 & 0 \\ 0 & 0 & \langle n_{a\uparrow}\rangle & 0 \\ 0 & 0 & 0 & \langle n_{b\uparrow}\rangle, \end{pmatrix}. \tag{3.11}$$

with the basis vector from equation 3.9. In the matrix representation the inter-site interaction in the mean-field approximation can be written as

$$H_V = z\ V \begin{pmatrix} \langle n_a\rangle & 0 & 0 & 0 \\ 0 & \langle n_b\rangle & 0 & 0 \\ 0 & 0 & \langle n_a\rangle & 0 \\ 0 & 0 & 0 & \langle n_b\rangle \end{pmatrix}, \tag{3.12}$$

with the basis vector shown in equation 3.9.

The Bloch Hamiltonian summed over the Brillouine zone gives the total energy and has the form

$$E^{MF} = \frac{1}{N_k} \sum_{\mathbf{k}} \phi_{\mathbf{k}}^{\dagger} (H_t + H_U + H_V) \phi_{\mathbf{k}} - E_0 \tag{3.13}$$

where N_k is the number of k points, the eigenvector $\phi_{\mathbf{k}}^{\dagger}$ from equation 3.9 and the constant energy E_0 is determined in equation 3.6. E_0 is only relevant for the calculation of the total energy and not for the following self-consistent calculations.

3.1 Band-Structures

The following band-structures are the tight-binding solutions for different lattices with no interactions. The lattices are divided into two sublattices A and B.

3.1.1 One-dimensional Lattice

The one-dimensional lattice is a bipartite lattice and divided into sublattices A and B as shown in 3.1, with a two-atom unit cell. The translation vector **T**

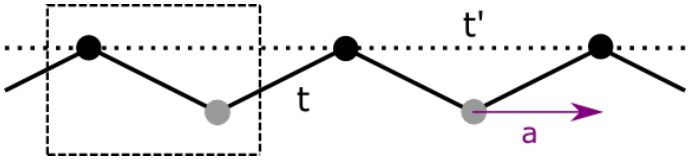

Figure 3.1: Schematic representation of the one-dimensional lattice with the primitive lattice vector $\mathbf{a_1}$, hopping constant t and second hopping constant t' and two atoms in the basis.

is composed of one primitive lattice vector

$$\mathbf{T} = n\mathbf{a_1}, \tag{3.14}$$

with the integer n and the primitive lattice vector

$$\mathbf{a_1} = a\hat{\mathbf{x}}, \tag{3.15}$$

with the lattice parameter a. The reciprocal lattice vector is

$$\mathbf{b} = \frac{2\pi}{a}\hat{\mathbf{x}}. \tag{3.16}$$

A site in the one dimensional lattice has two nearest neighbours, the coordination number is $z = 2$. The vectors for those nearest neighbours in real space can be written as

$$\delta_1 = \mathbf{a_1}, \delta_2 = -\mathbf{a_1}. \tag{3.17}$$

And there are two next nearest neighbours at the one dimensional lattice. The vectors for the next nearest neighbours are

$$\delta_1' = 2\mathbf{a_1}, \delta_2' = -2\mathbf{a_1}. \tag{3.18}$$

The hopping part for the one-dimensional Hamiltonian with the nearest neighbours in equation 3.17 and the next-nearest neighbours in equation 3.18 inserted into equation 3.7 gives the matrix

$$H_{t'} = \begin{pmatrix} g_k' & g_k^* \\ g_k & g_k' \end{pmatrix}, \tag{3.19}$$

with the neighbour term

$$g_k = -t(1 + e^{i2ak_x}) \tag{3.20}$$

and the second neighbour term

$$g_k' = 2t' \cos(2ak_x). \tag{3.21}$$

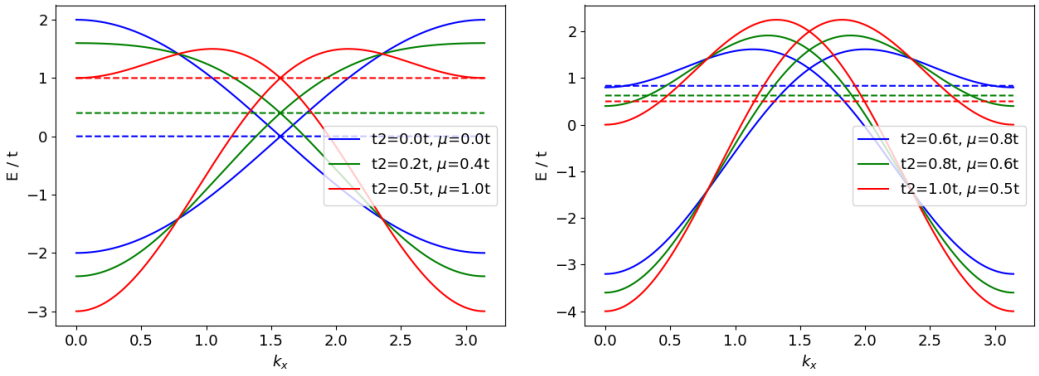

Figure 3.2: Energy dispersion of the one-dimensional lattice with a two-atom unit cell and different next neighbour hopping constants t'. The dashed lines mark the chemical potential for the different hopping constants.

The diagonalized Matrix 3.19 gives two energy bands

$$\epsilon_k'^{\pm} = 2t' \cos(2ak_x) \pm 2t \cos(ak_x). \tag{3.22}$$

Figure 3.2 shows the energy bands for different next nearest neighbour transfers t'/t and the according chemical potential μ. The particle-hole symmetry breaks with the increase of the second hopping t'/t and the density of states becomes progressively asymmetric.

3.1.2 Cubic Lattice

The cubic lattice is represented in figure 3.3, where the lattice constant a between the sites and the hopping constants t and t' can be seen. The lattice is a bipartite lattice and divided into sublattices A and B, with two-atoms in the unit cell. The translation vector $\mathbf{T}$ is composed of two primitive vectors

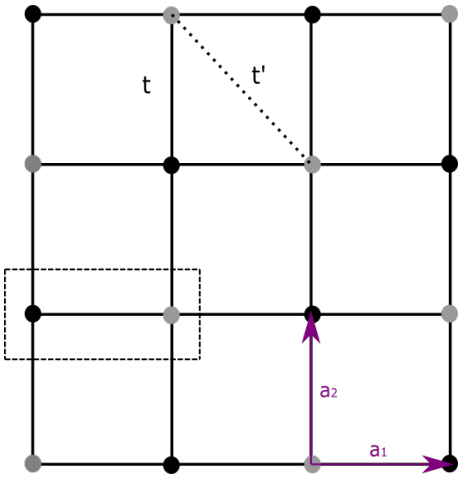

Figure 3.3: Two-Dimensional square lattice with the primitive lattice vectors $\mathbf{a_1}$ and $\mathbf{a_2}$, the hopping constants t and t' and two atoms in the basis.

$$\mathbf{T} = n\mathbf{a_1} + m\mathbf{a_2} \tag{3.23}$$

where n and m are integers and the primitive lattice vectors are

$$\begin{aligned} \mathbf{a_1} &= a\hat{\mathbf{x}} \\ \mathbf{a_2} &= a\hat{\mathbf{y}}. \end{aligned} \tag{3.24}$$

a is the lattice constant for the distance between the basis atoms. The reciprocal lattice vectors are

$$\begin{aligned} \mathbf{b_1} &= \frac{2\pi}{a}\hat{\mathbf{x}} \\ \mathbf{b_2} &= \frac{2\pi}{a}\hat{\mathbf{y}}. \end{aligned} \tag{3.25}$$

In the square lattice are four nearest neighbours and the coordination number is $z = 4$. The vectors in real space for the nearest neighbours are

$$\begin{aligned} \boldsymbol{\delta_1} = \mathbf{a_1},\ \boldsymbol{\delta_2} = -\mathbf{a_1} \\ \boldsymbol{\delta_3} = \mathbf{a_2},\ \boldsymbol{\delta_4} = -\mathbf{a_2}. \end{aligned} \tag{3.26}$$

The vectors for the four next nearest neighbours can be written as

$$\begin{aligned} \boldsymbol{\delta_1'} = \mathbf{a_1} + \mathbf{a_2},\ \boldsymbol{\delta_2'} = -\mathbf{a_1} - \mathbf{a_2} \\ \boldsymbol{\delta_3'} = \mathbf{a_2} - \mathbf{a_2},\ \boldsymbol{\delta_4'} = -\mathbf{a_1} + \mathbf{a_2}. \end{aligned} \tag{3.27}$$

The hopping part of the Hubbard Hamiltonian on the square lattice with nearest and next nearest neighbours is

$$H_{t'} = \begin{pmatrix} g_k' & g_k^* \\ g_k & g_k' \end{pmatrix} \tag{3.28}$$

with the neighbour hopping term

$$g_k = -t[1 + e^{-i2ak_x} + e^{-ia(k_x+k_y)} + e^{-ia(k_x-k_y)}]. \tag{3.29}$$

and the next-neighbour hopping term

$$g_k' = 4t' \cos(ak_x) \cos\big(ak_y\big). \tag{3.30}$$

With the diagonalization of the Matrix 3.28 two energy bands can be found

$$\epsilon_k^{\pm} = 4t' \cos(ak_x) \cos\big(ak_y\big) \pm 2t(\cos(ak_x) + \cos\big(ak_y\big)). \tag{3.31}$$

Figure 3.4 and 3.5 show the energy bands $E_k^{\pm}$ for the square lattice. In figure 3.4 only direct hopping is taken into account and the second hopping constant is zero $t'/t = 0$. The particle-hole symmetry is valid and perfect nesting can be found. In figure 3.5 the second hopping is included with $t'/t = 0.2$. The particle-hole symmetry is broken and bands become asymmetric. There is a loss of perfect nesting.

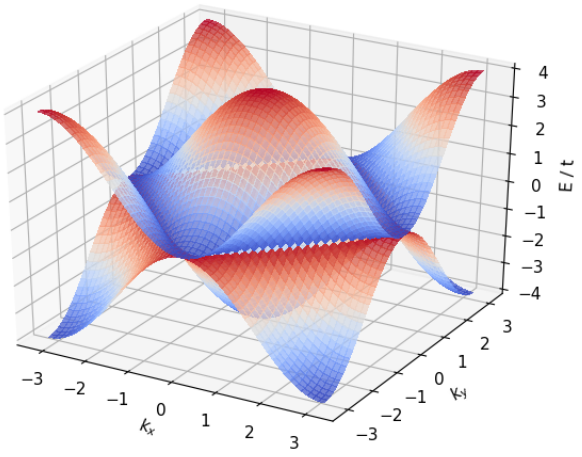

Figure 3.4: The energy dispersion of the square lattice with $t'/t = 0$ and a particle-hole symmetry.

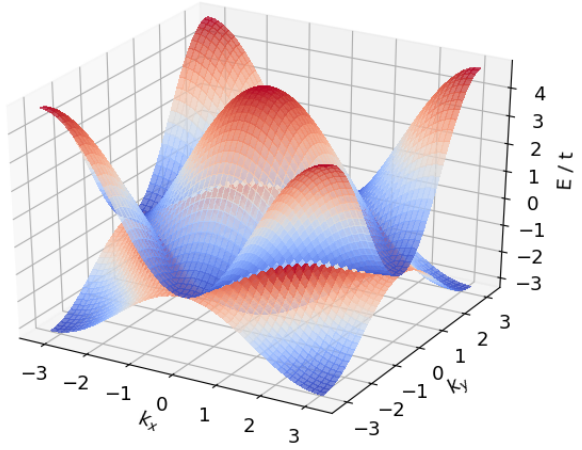

Figure 3.5: The energy dispersion of the square lattice with $t'/t = 0.2$ and a broken particle-hole symmetry.

The density of states of the square lattice can be seen in figure 3.6, on the left side for $t'/t = 0$ and on the right side for $t'/t = 0.2$. The two colours, blue and orange, represent the two partially filled bands. The density of

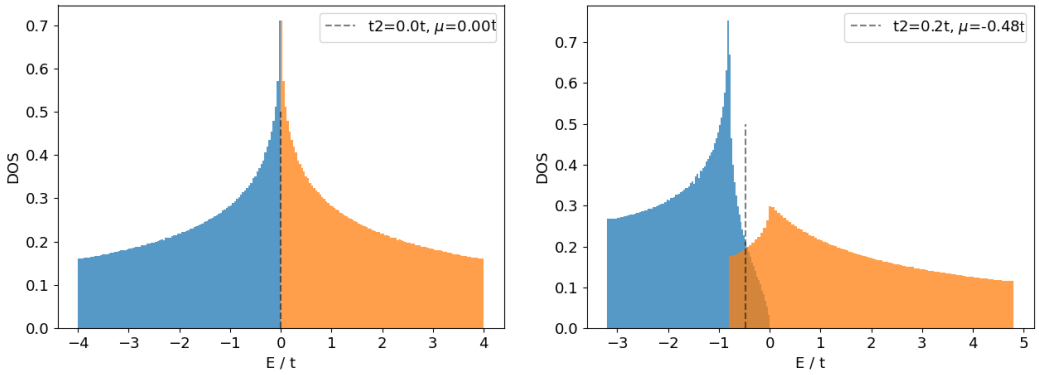

Figure 3.6: Density of states for a square lattice symmetric for $t'/t = 0$ with $\mu = 0.0t$ on the left and asymmetric for $t'/t = 0.2$ with $\mu = -0.5t$ on the right. The blue and the orange colours represent the two partially filled band.

states displays a logarithmic singularity for small energies. From topological arguments, as discussed in [7], the singularity will always occur in a two-dimensional system. For the nearest neighbour hopping model, it is a special case that the singularity occurs at the Fermi energy. This is only valid for the energy where perfect nesting occurs.

3.1.3 Honeycomb Lattice

The honeycomb lattice itself is not a Bravais lattice. The Bravais lattice of the honeycomb lattice is the hexagonal lattice with a basis of two atoms per unit cell, as shown in figure 3.7. The bipartite lattice is again divided into the sublattices A and B. The translation vector $\mathbf{T}$ of the hexagonal lattice is

$$\mathbf{T} = n\mathbf{a_1} + m\mathbf{a_2}, \tag{3.32}$$

with the integers n and m. The primitive lattice vectors can be written as

$$\begin{aligned} \mathbf{a_1} &= \frac{a}{2}\hat{\mathbf{x}} + \frac{\sqrt{3}a}{2}\hat{\mathbf{y}} \\ \mathbf{a_2} &= -\frac{a}{2}\hat{\mathbf{x}} + \frac{\sqrt{3}a}{2}\hat{\mathbf{y}}, \end{aligned} \tag{3.33}$$

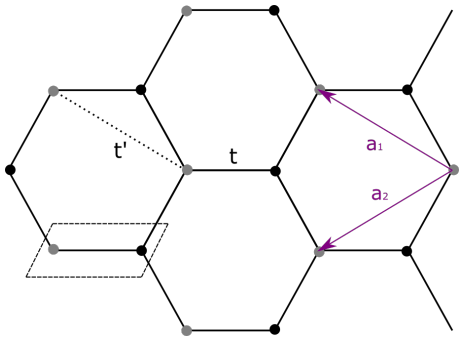

Figure 3.7: Two Dimensional honeycomb lattice with the primitive lattice vectors $\mathbf{a_1}$ and $\mathbf{a_2}$, the hopping constants t and t' and two atoms in the basis.

with the lattice constant a. The reciprocal lattice vectors are given by

$$\begin{aligned} \mathbf{b_1} &= -\frac{2\pi}{a}\hat{\mathbf{x}} + \frac{2\pi}{\sqrt{3}a}\hat{\mathbf{y}} \\ \mathbf{b_2} &= \frac{2\pi}{a}\hat{\mathbf{x}} + \frac{2\pi}{\sqrt{3}a}\hat{\mathbf{y}}. \end{aligned} \tag{3.34}$$

The coordination number of the honeycomb lattice is $z = 3$. The three nearest neighbours in real space are given by the vectors

$$\begin{aligned} \boldsymbol{\delta_1} &= \frac{a}{2}\hat{\mathbf{x}} + \frac{a}{2\sqrt{3}}\hat{\mathbf{y}} \\ \boldsymbol{\delta_2} &= -\frac{a}{2}\hat{\mathbf{x}} + \frac{a}{2\sqrt{3}}\hat{\mathbf{y}} \\ \boldsymbol{\delta_3} &= -\frac{a}{\sqrt{3}}\hat{\mathbf{y}}, \end{aligned} \tag{3.35}$$

and the six next nearest neighbours are located at

$$\begin{aligned} \boldsymbol{\delta'_{1,2}} &= \pm\mathbf{a_1}, \boldsymbol{\delta'_{3,4}} = \pm\mathbf{a_2} \\ \boldsymbol{\delta'_{4,5}} &= \pm(\mathbf{a_2} - \mathbf{a_1}). \end{aligned} \tag{3.36}$$

With the same method as above for the other two lattices, but with the according Brillouin zone, the hopping term is

$$H_{t'} = \begin{pmatrix} g'_k & g^*_k \\ g_k & g'_k \end{pmatrix}, \tag{3.37}$$

with the nearest neighbour hopping term

$$g_k = -t[e^{i\frac{ak_y}{\sqrt{3}}} + 2cos(\frac{ak_x}{2})e^{-i\frac{ak_y}{2\sqrt{3}}}] \tag{3.38}$$

and the next-nearest neighbour hopping term

$$g'_k = t'[4cos(\frac{ak_x}{2})cos(\frac{\sqrt{3}ak_y}{2}) + 4cos^2(\frac{ak_x}{2}) - 2]. \tag{3.39}$$

The energy bands derived from the Hubbard Hamiltonian of the honeycomb lattice have the form [13,14]

$$\begin{aligned}\epsilon_k^{\pm} =& t'[4cos(\frac{ak_x}{2})cos(\frac{\sqrt{3}ak_y}{2}) + 4cos^2(\frac{ak_x}{2}) - 2] \\ &\pm t\sqrt{1 + 4cos(\frac{ak_x}{2})cos(\frac{\sqrt{3}ak_y}{2}) + 4cos^2(\frac{ak_x}{2})}.\end{aligned} \tag{3.40}$$

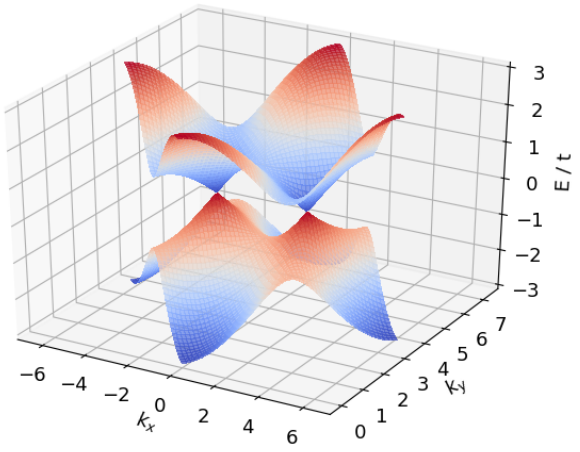

Figure 3.8: The energy dispersion of the honeycomb lattice for $t'/t = 0.0$. The dispersion has particle-hole symmetry.

The honeycomb lattice has two important points at the corners of the Brillouin zone, K and K', as explained in [14]. These points are named Dirac

points and are of particular importance for the physics of the honeycomb lattice. Their positions given in momentum space are

$$\mathbf{K} = \left(-\frac{2\pi}{3a}, \frac{2\pi}{3\sqrt{3}a}\right), \mathbf{K}' = \left(\frac{2\pi}{3a}, \frac{2\pi}{3\sqrt{3}a}\right). \tag{3.41}$$

The Fermi surface reduces to points at the Dirac points. The density of states is negligible and the material is a semimetal, as shown in [15].

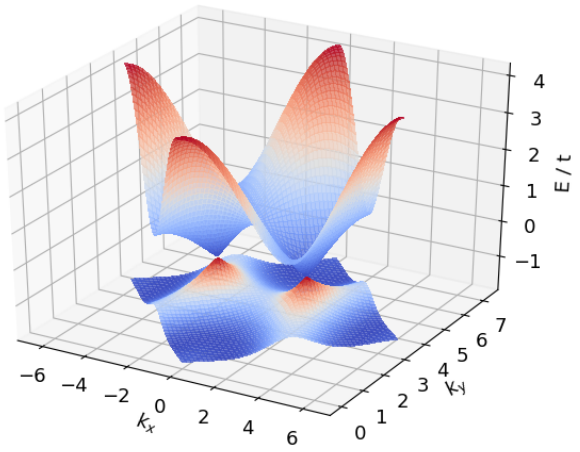

Figure 3.9: The energy dispersion of the honeycomb lattice for $t'/t = 0.2$. The figure shows a broken particle-hole symmetry.

Figure 3.8 shows the energy dispersion of the honeycomb lattice without next-nearest neighbour hopping $t'/t = 0.0$. The dispersion has a particle-hole symmetry. Figure 3.9 shows the energy dispersion with included next-nearest neighbour hopping with the hopping constant $t'/t = 0.2$. For finite values of t' the particle-hole symmetry is broken and the π and π^* bands become asymmetric. The presence of next-neighbour hopping t' shifts the position of the Dirac points in energy and breaks the symmetry.

The density of states of the honeycomb lattice has the form shown in figure 3.10. For $t'/t = 0$ the Van Hoove singularities are at the energies $\pm t = \pm 1$. The density of states decreases to zero at the Fermi level. With the inclusion of the next-nearest neighbour hopping $t'/t = 0.2$, the density of states loses

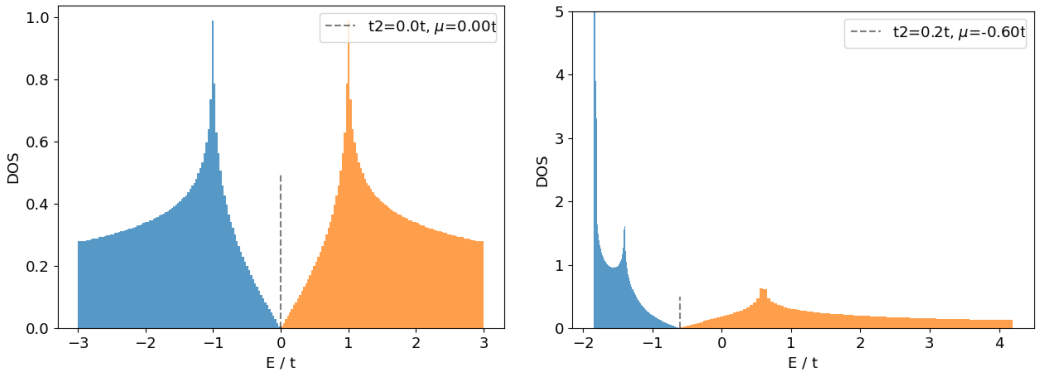

Figure 3.10: Density of states per unit cell calculated from the energy dispersion, $t'/t = 0.0$ with $\mu/t = 0.0$ on the left and $t'/t = 0.2$ with $\mu/t = -0.6$ on the right. The dashed line mark the chemical potential and the orange and blue colors represent the two bands.

its symmetry. The figure shows the two bands in the colors blue and orange and the chemical potential is marked with a dashed line.

3.2 Self-consistent Calculation

In the self-consistent calculations, the tight-binding solution for the different lattices, shown in the previous section, is combined with the Coulomb interactions in the Hubbard Hamiltonian. The density parameters $\langle n_{A_\downarrow} \rangle$, $\langle n_{A_\uparrow} \rangle$, $\langle n_{B_\downarrow} \rangle$ and $\langle n_{B_\uparrow} \rangle$ can be found in this process and the ground state of the system can be determined.

The start is a guess of the initial values of the density parameters, where

$$\sum_i \langle n_{i_\sigma} \rangle = N_e, \tag{3.42}$$

with N_e the number of electrons. In this work the number of electrons is $N_e = 2$. This initial guess is important for the result, because for example an initial paramagnetic state will stay paramagnetic during the calculation. The next step is the calculation of the Hamiltonian with the density parameters to find the energies of the bands. The ground state of the system can be

found and the chemical potential can be determined. The density values of the ground state are calculated with equation 2.36 at the limit $T \to 0$, which gives

$$\langle n_{i_\sigma} \rangle = \frac{1}{N_k} \sum_{\mathbf{k},m} \Theta(\mu - E_{m\mathbf{k}}) |u_{m\mathbf{k}}|^2, \tag{3.43}$$

with the chemical potential μ, the energy $E_{m\mathbf{k}}$ and the occupied eigenstates $u_{m\mathbf{k}}$. The notation i stands for the different atom types A and B. The Theta function, or step function, is in this case defined as

$$\Theta(\mu - \epsilon_{m\mathbf{k}}) = \begin{cases} 0 & \text{if } \mu < \epsilon_{m\mathbf{k}} \text{the energy is above the chemical potential,} \\ 1 & \text{if } \mu \geq \epsilon_{m\mathbf{k}} \text{ the energy is below the chemical potential.} \end{cases} \tag{3.44}$$

The step function is important, because of the broken particle-hole symmetry and the shifted chemical potential. The new density values serve in the calculation of the next Hamiltonian for the next determination of the ground state. This procedure is iterated until convergence of the electron densities is achieved.

Oscillation or numerical instabilities can delay or destroy the convergence. The easiest solution for this problem is simple mixing

$$m_i = k m_i + (1 - k) m_{i-1}, \tag{3.45}$$

where the self-consistent parameter m_i of the iteration i gets mixed with the parameter m_{i-1} of the iteration $i - 1$ and the mixing parameter k is in the range $[0, 1]$. The typical value for k is around 0.7.

Another self-consistency relation for systems in the absence of inter-site interactions, $V = 0$, holds for the antiferromagnetic magnetization m_{AF}

$$m_{AF} = \frac{2}{N_k} \sum_{\mathbf{k}} \frac{m_{AF} U}{\sqrt{(E_{\mathbf{k}} - E_{\mathbf{k}+\mathbf{Q}})^2 + m_{AF}^2 U^2}}, \tag{3.46}$$

with N_k the number of sites. The deviation of this formula can be found in [7]. At half filling the perfect nesting condition is $E_{\mathbf{k}} = -E_{\mathbf{k}+\mathbf{Q}}$ for a square lattice. Equation 3.46 shows that all $m_{AF} \neq 0$ for all values of $U > 0$ at perfect nesting. The system becomes unstable with respect to the formation of antiferromagnetic ordering.

3.3 Energy

The mean-field matrix decouples into two 2x2 matrices. The analytical solution for the calculation of the energy bands is

$$\begin{aligned} E^{\pm}_{\sigma\mathbf{k}} = &\frac{U(\langle n_{i\sigma}\rangle + \langle n_{j\sigma}\rangle)}{2} + zV + g_{k'} \\ &\pm \sqrt{g_k^2 + \frac{1}{4}[U(\langle n_{i\sigma}\rangle - \langle n_{j\sigma}\rangle) + zV(-\langle n_i\rangle + \langle n_j\rangle)]^2}. \end{aligned} \tag{3.47}$$

The total energy derived from equation 3.13 at half filling is

$$\begin{aligned} E_{tot} = &\frac{1}{N_k}\sum_k (E^{\pm}_{\sigma\mathbf{k}}\Theta(\mu - E^{\pm}_{\sigma\mathbf{k}}) \\ &- U(\langle n_{i\uparrow}\rangle\langle n_{i\downarrow}\rangle) + \langle n_{j\uparrow}\rangle\langle n_{j\downarrow}\rangle) - zV(\langle n_i\rangle\langle n_j\rangle), \end{aligned} \tag{3.48}$$

where the Θ-function $\Theta(\mu - E^{\pm}_{\mathbf{k}\sigma})$ ensures that only the filled states are taken into account for the energy. This measure is necessary because of the broken particle-hole symmetry.

The orderings described in section 2.4 are related to order parameters and can be expressed as a function of the densities.

i) *paramagnetic ordering* The densities in paramagnetic ordering take the form

$$\langle n_{i\uparrow}\rangle = \langle n_{i\downarrow}\rangle = \frac{1}{2}\rho, \tag{3.49}$$

with the filling $\rho = 1$ at the half filled case. The band energies simplify to

$$E^{\pm,(para)}_{\mathbf{k}} = \frac{U}{2} + zV + g_{k'} \pm g_k. \tag{3.50}$$

where the spin σ of the band does not influence the solution.

ii) *SDW ordering* The antiferromagnetic state, which is a special form of the spin-density wave at half filling, is described by densities in the form of

$$\begin{aligned} \langle n_{a\uparrow} \rangle &= \langle n_{b\downarrow} \rangle \\ \langle n_{a\uparrow} \rangle &\neq \langle n_{a\downarrow} \rangle. \end{aligned} \tag{3.51}$$

The SDW energy bands simplify to

$$E_{\sigma\mathbf{k}}^{\pm,(SDW)} = \frac{U}{2} + zV + g_{k'} \pm \sqrt{g_k^2 + \frac{U^2}{4}(\langle n_{a\sigma} \rangle - \langle n_{b\sigma} \rangle)^2}. \tag{3.52}$$

To describe the level of antiferromagnetic ordering, the parameter m_{AF} is introduced

$$m_{AF} = \langle n_{a\uparrow} \rangle - \langle n_{a\downarrow} \rangle - \langle n_{b\uparrow} \rangle + \langle n_{b\downarrow} \rangle, \tag{3.53}$$

where at half filling m_{AF} can take the values $-2 \leq m_{AF} \leq 2$. If the lattice points A and B are exchanged, the parameter changes its sign. Accordingly the future findings are presented as the absolute value $|m_{AF}|$.

iii) *CDW ordering* The densities of the charge-density wave behave like

$$\begin{aligned} \langle n_{a\uparrow} \rangle &= \langle n_{a\downarrow} \rangle \\ \langle n_{a\uparrow} \rangle &\neq \langle n_{b\uparrow} \rangle. \end{aligned} \tag{3.54}$$

The CDW energy bands are

$$\begin{aligned} E_{\sigma\mathbf{k}}^{\pm,(CDW)} = &\frac{U(\langle n_{a\sigma} \rangle + \langle n_{b\sigma} \rangle)}{2} + zV + g_{k'} \\ &\pm \sqrt{g_k^2 + \frac{1}{4}[U(\langle n_{a\sigma} \rangle - \langle n_{b\sigma} \rangle) + zV(-\langle n_a \rangle + \langle n_b \rangle)]^2} \end{aligned} \tag{3.55}$$

of the charge-density waves is made by the sublattice difference parameter Δ_{AB}

$$\Delta_{AB} = -\langle n_{a\uparrow} \rangle - \langle n_{a\downarrow} \rangle + \langle n_{b\uparrow} \rangle + \langle n_{b\downarrow} \rangle, \tag{3.56}$$

where the solution gives the occupation of the sublattices. For the same reason as above the future findings are presented as an absolute value $|\Delta_{AB}|$.

iv) ferromagnetic ordering The densities of the ferromagnetic ordering have the form

$$\begin{aligned} \langle n_{a\uparrow} \rangle &= \langle n_{b\uparrow} \rangle \\ \langle n_{a\uparrow} \rangle &\neq \langle n_{a\downarrow} \rangle \end{aligned} \tag{3.57}$$

The energy band calculation of the ferromagnetic ordering can be simplified to

$$E^{\pm,(ferro)}_{\sigma\mathbf{k}} = \frac{U(\langle n_{a\sigma} \rangle + \langle n_{b\sigma} \rangle)}{2} + zV + g_{k'} \pm g_k. \tag{3.58}$$

The level of ferromagnetic ordering can be described by the parameter m_F

$$m_F = \langle n_{a\uparrow} \rangle - \langle n_{a\downarrow} \rangle + \langle n_{b\uparrow} \rangle - \langle n_{b\downarrow} \rangle \tag{3.59}$$

where this magnetisation does not occur for half-filling. Ferromagnetism can be found for very high interaction parameter and close to the half filling as shown in [9]. Ferromagnetism is not under consideration for this work and is only listed for completeness.

The following phase diagrams and transitions are obtained by choosing the solution that gives the lowest energy, if more than one solution exists.

3.4 Results for ordered Phases and Phase diagrams

The following sections show the results with only nearest neighbour hopping $t'/t = 0$ and with the inclusion of next-nearest neighbour hopping $t'/t \neq 0$.

3.4.1 NN hopping $t'/t = 0$

Antiferromagnetic bands are characterized by an opening of a gap G, which leads to the insulation phase. This gap is not related to the metal-insulator transition of the Mutt-Hubbard kind, as it is not related to the electronic correlations, but to magnetism.

There is a clear symmetry at half filling, with no next-neighbour hopping. The ground state of non-interacting electrons ($U, V = 0$) is in a paramagnetic state. The minimum energy constraint in combination with the Pauli principle forces to fill all the energy levels from the lowest to the highest with an equal number of spin up and spin down electrons. For large interactions U the electrons take advantage of hopping by hopping back and forth between neighbouring sites. The Pauli principle demands that this process can only take place, if the neighbouring electrons have opposite spins. This results in antiferromagnetic correlations between sites, as explained in [8]. The so called t-J model demonstrates this correlations well.

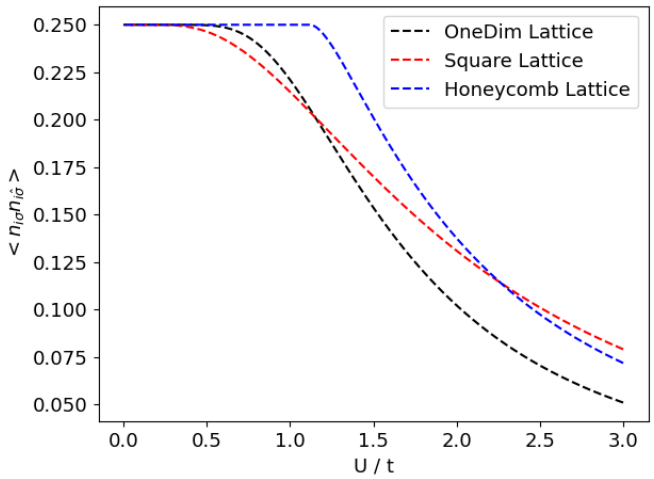

Figure 3.11: Suppression of the doubly occupied sites as a function of U, with $V = 0$, for three different lattices.

Figure 3.11 shows how the configurations with doubly occupied states get reduced with rising on-site interaction U for the different lattices.

It can be seen, that the one dimensional and square lattice have a stronger tendency to antiferromagnetic ordering in comparison to the honeycomb lattice. The reason for this behaviour is in the nesting condition, which is fulfilled for the two lattices, as explained in section 2.3.1.

One-dimensional Lattice

The one dimensional lattice shows a spin-density wave ordering with increasing on-site interaction and a charge-density wave ordering with increasing inter-site interaction. This behaviour is expected and can be seen in figure 3.12. The critical value for the phase transition between the metallic phase and spin-density wave phase is $U_c = 0.58t$ for $V = 0$. This value can also be found it other literature [16]. The perfect nesting condition would expect this value to be zero, but since we use a small but finite epsilon, below which we interpret the order parameter and the gap to be zero, this finite value was found. The charge-density wave ordering shows a phase transition at the critical value $zV_c = 0.29t$ for $U = 0$. It can be seen that $zV_c \approx \frac{U_c}{2}$. Figure 3.12 additionally shows the according gap size of the two transitions on the right scale of the plots.

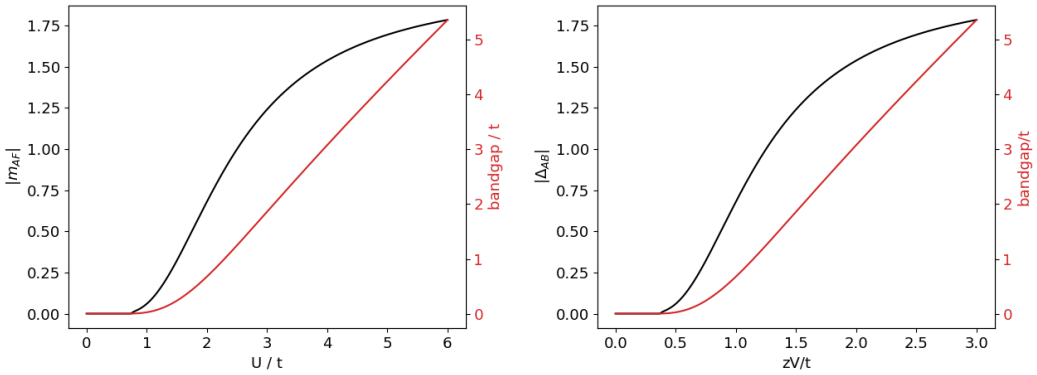

Figure 3.12: Magnetism m_{AF} for the one dimensional lattice with a critical on-site interaction U and the according gap size with $V = 0$ on the left and the sublattice difference Δ_{AB} as a function of the inter-site interaction V and the according gap size with $U = 0$ on the right.

Square Lattice

The square lattice also shows charge-density wave and spin-density wave ordering for the increasing interactions. The phase transition from the paramagnetic to the SDW and CDW orders is a second order transition. The

critical value of $U_c = 0.38$ for $V = 0$ is similar to the one obtained in other literature [7].The theoretical value for this transition is zero, because of the nesting. The nesting of the Fermi surface and the Van Hove singularity in the density of states occur at the same energy, the Fermi energy for the half filled case. The gap in the square lattice for the antiferromagnetic ordering has a special form because of the singularity at the Fermi energy. Equation 2.33 simplifies according to [7] to

$$G_{SQ} \sim te^{-2\pi\sqrt{t/U}} \tag{3.60}$$

and because of the relation $G \sim m_{AF}U$, the magnetization can be written as

$$m_{AF} \sim \frac{t}{U} e^{-2\pi\sqrt{t/U}}. \tag{3.61}$$

Figure 3.13 shows that the magnetization has identical behaviour as theoretically shown in equation 3.61. The equations imply that U_c should be zero. This exponential growth of the gap is almost impossible to resolve in numerical calculations, that is why we infer a critical value U_c which is greater than zero from the numerics.

Figure 3.14 shows identical behaviour as theoretically shown in equation 3.60.

The charge-density wave ordering shows a transition at the critical value $zV_c = 0.19t$ for $U = 0$. The critical values have the relation $zV_c = \frac{U_c}{2}$. Figure 3.15 shows the sublattice difference Δ_{AB} for the charge-density wave on the left and a plot of the energy bands for the interaction values $U = 3t$ and $zV = 1$ on the right.

Honeycomb Lattice

The honeycomb lattice has no nesting at the Fermi surface and the phase transitions have a different behaviour compared to the one dimensional and square lattice transitions. The transition between the paramagnetic and the antiferromagnetic phase is very sharp.

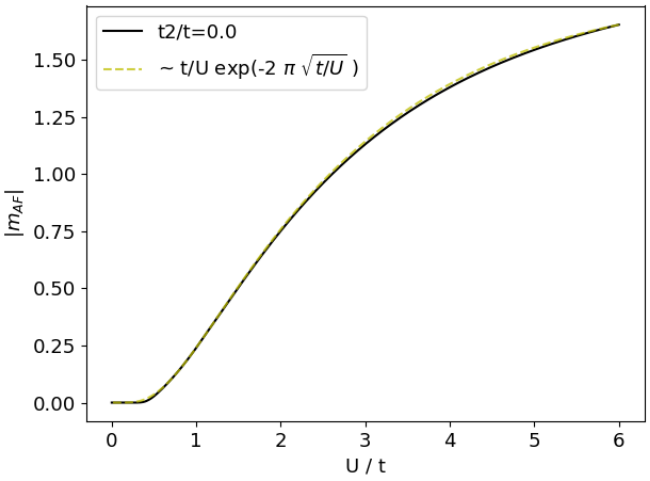

Figure 3.13: Magnetism m_{AF} for the square lattice as a function of the on-site interaction U with $V = 0$. The function is compared to the theoretical values from equation 3.61.

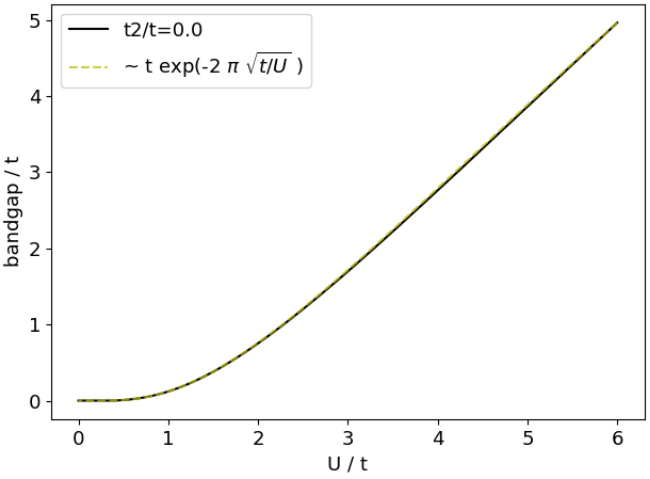

Figure 3.14: Gap size for the square lattice as a function of the on-site interaction U with $V = 0$. The function is compared to the theoretical values from equation 3.60.

For the honeycomb lattice, the critical value for the transition of the on-site interaction is $U_c = 2.25t$ with $V = 0$. This value can also be found in

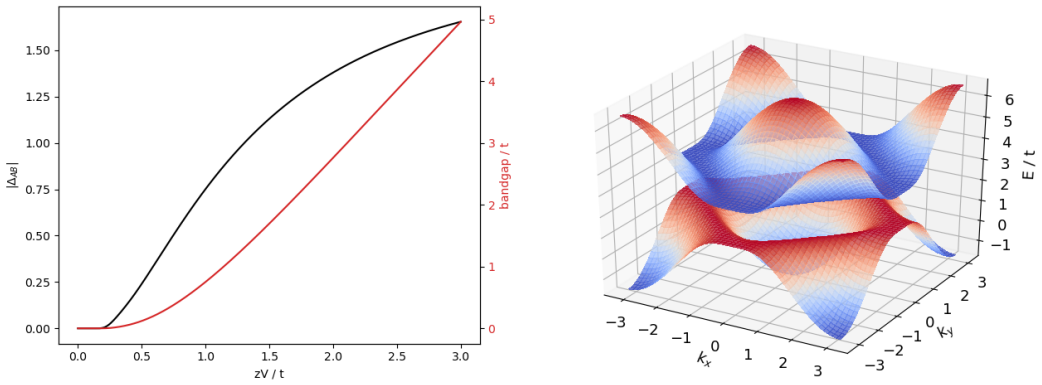

Figure 3.15: Sublattice difference Δ_{AB} for the square lattice as a function of the inter-side interaction zV with $U = 0$ on the left and on the right the dispersion relation at the values $U = 3t$ and $zV = 1t$.

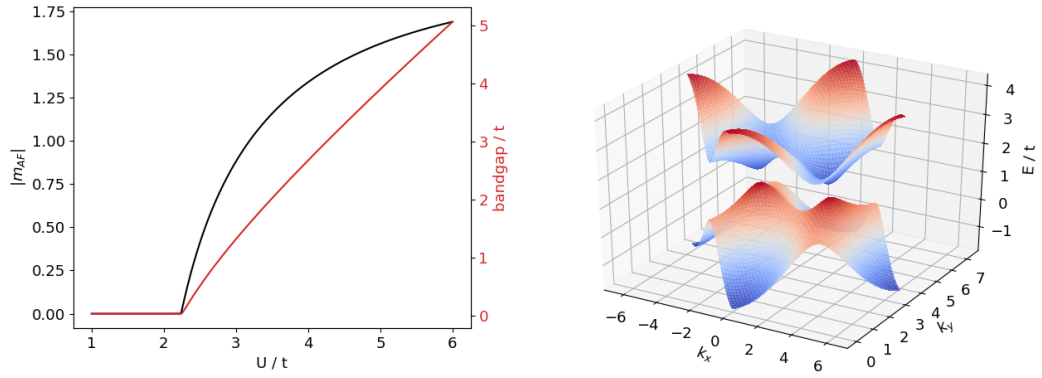

Figure 3.16: The transition between paramagnetic and spin-density wave ordering for the honeycomb lattice can be seen on the right. The transition occurs on a critical on-site interaction $U_c = 2.30t$. The left side shows the dispersion relation at the value $U = 2.5t$. The inter-site value is zero $V = 0$ for both plots.

other literature [14]. Figure 3.16 shows the transition in the form of the antiferromagnetic magnetisation m_{AF} as a function of the on-site interaction U on the left. The right figure is the dispersion relation for a interaction of $U = 2.5t$ at $V = 0$.

The critical value for the charge-density wave transition is $zV_c = 1.12t$ with $U = 0$. The critical values have again the relation $zV_c = \frac{U_c}{2}$. Figure 3.17

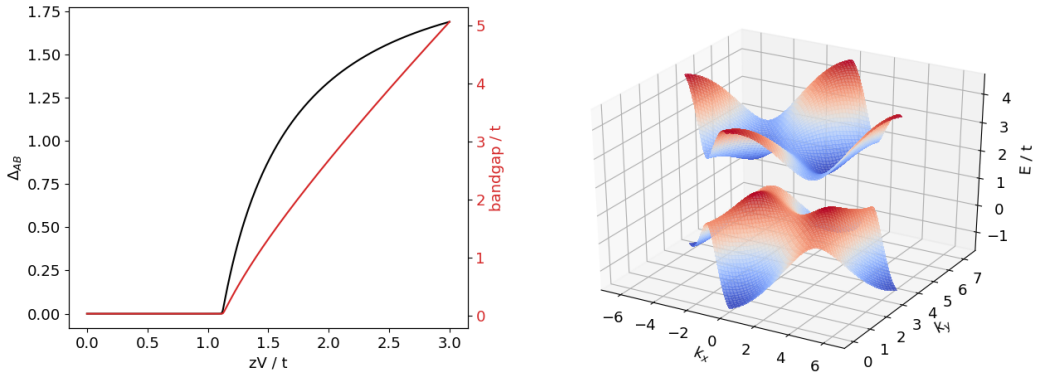

Figure 3.17: Charge-density wave for the honeycomb lattice with a critical inter-site interaction $zV_c = 1.12t$ on the left and on the right the dispersion relation at the value $zV = 1.5t$, with $U = 0$ for both plots.

shows the transition of the charge-density wave to the paramagnetic phase in form of the sublattice difference as a function to the inter-site interaction V on the left and the energy distribution at an interaction of $zV = 1.5t$, with $U = 0$ for both plots.

3.4.2 NN and NNN hopping $t'/t \neq 0$

Only the on-site interaction U was taken into account for the following calculations. The inter-site interaction was taken to be zero $V = 0$.

One-dimensional Lattice

The tight-binding energy in the one dimensional case is

$$E_{\mathbf{k}} = E_0 + 2t'cos(2ak_x) - 2tcos(ak_x) \tag{3.62}$$

with the constant $E_0 = 0$. The surface in the first Brillouin zone where $E_{\mathbf{k}} = 0$ is the Fermi Surface. For the $t'/t = 0$ case, the reciprocal vector for perfect nesting is $\pi/2a$, as explained in section 2.3.1. For the case $t'/t \neq 0$

there is still perfect nesting, if the chemical potential has the value $\mu = 2t'/t$, because

$$E_{\frac{\pi}{2a}} = -2t'. \tag{3.63}$$

The chemical potential of the one dimensional lattice for half filling has the value $\mu = 2t'/t$. This is valid for values between $0.0 \leq t'/t \leq 0.5$, as shown in figure 3.18. Therefore there is perfect nesting in the one dimensional lattice at half filling and the gap size for all values of $U > 0$ is the same for the different hopping values $t'/t < 0.5$.

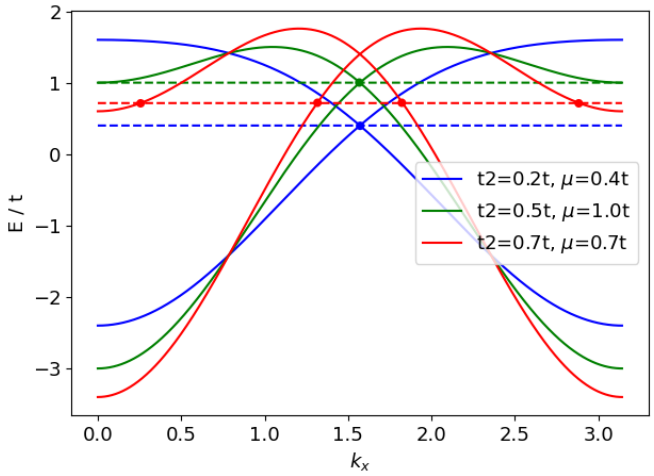

Figure 3.18: Band structure for the hopping constants $t'/t = [0.2, 0.5, 0.7]$ of the one-dimensional lattice. There is a change in the Fermi surface for $t' \geq 0.5$ and a loss of perfect nesting occurs.

For a values $t'/t > 0.5$ the chemical potential differs from $2t'/t$. There are more than one Fermi points, shown in figure 3.18, because of the changing band structure topology, and a loss of perfect nesting occurs.

Figure 3.19 shows the antiferromagnetic parameter and figure 3.20 shows the gap sizes for the one-dimensional lattice at different values t'/t.

The gap size jumps to zero discontinuously with the reduction of the Coulomb interaction U below the critical value $U_c(t')$. This indicates a first order transition. For an interaction $U > U_c$ the gap behaves like the gap for $t' = 0$. The critical transition values $U_c(t')$ of the transition as a function

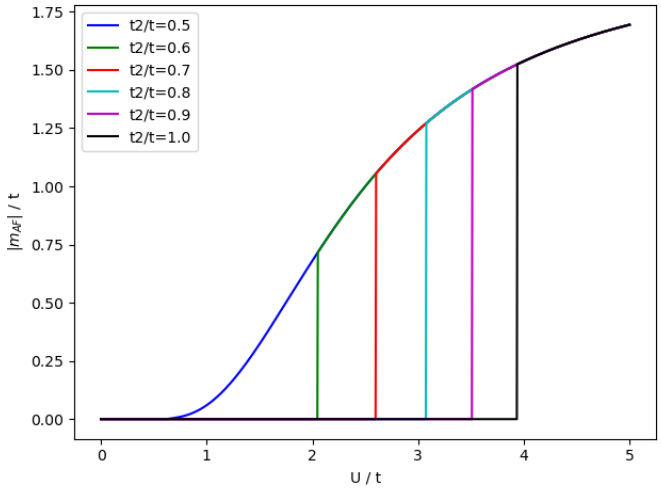

Figure 3.19: One-dimensional lattice antiferromagnetic parameter m_{AF} as a function of the on-site interaction U for different values $t'/t \geq 0.5$.

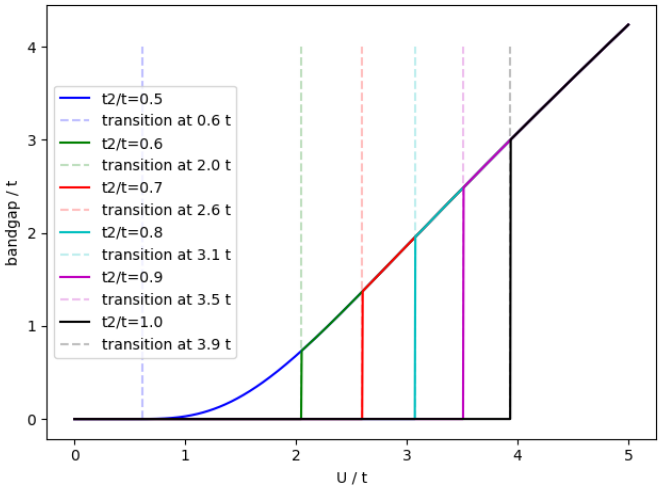

Figure 3.20: One dimensional lattice gap size for different values $t'/t \geq 0.5$. The dashed lines indicate the phase transitions.

of the hopping constant t' is shown in figure 3.21. The values up to the threshold $t'_s/t = 0.5$ are $U_c(t') = 0.58$.

The values beyond $t' > t'_s$ have an asymptotic behaviour. U_c decreases very

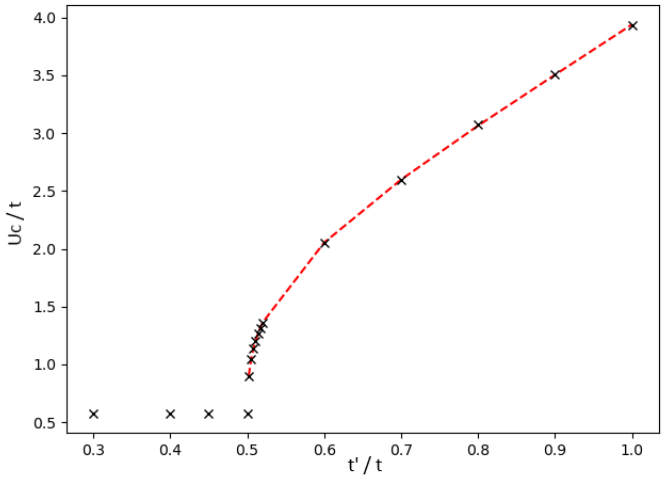

Figure 3.21: Critical value U_c as a function of the hopping t'/t with an asymptotic behaviour for $t'/t \to 0.5$.

fast for $t' \to t'_s$. A fitted description of the asymptotic behaviour is

$$[U_c(t')]^{-1} = \frac{c_1}{2} \ln(t')^2 + c_2 \ln(t') + c_3 \tag{3.64}$$

with the values $c_1 = 0.01$, $c_2 = -0.14$ and $c_3 = 0.16$ an $t'/t > 0.5$.

The critical transition values $U_c(t')$ can be found in table 3.1.

Table 3.1: Critical transition values $U_c(t')$ for the different next-nearest neighbour hopping constants t' for the one-dimensional lattice.

t'/t	$U_c(t')/t$
0.5	0.6
0.6	2.0
0.7	2.6
0.8	3.1
0.9	3.5
1.0	3.9

Square Lattice

The square lattice has no perfect nesting for any $t' \in (0, 5t]$ at half filling and consequently $t'_s = 0$. Figure 3.22 shows the antiferromagnetic parameter m_{AF} as a function of U for different hopping constants on the left. On the right hand side, the size of the band gap is shown for different t' with the critical transition values $U_c(t')$. This solutions can also be found in other literature [11][12].The gap size jumps discontinuously to zero, if the Coulomb interaction U is reduced below the critical value $U_c(t')$. This is again a first order transition. Table 3.2 shows the critical transition values $U_c(t')$ for the different t' constants.

Table 3.2: Critical transition values $U_c(t')$ for the different next-nearest neighbour hopping constants t' for the square lattice.

t'/t	$U_c(t')/t$
0.0	0.4
0.1	1.5
0.2	2.0
0.3	2.5
0.4	2.9
0.5	3.2

Figure 3.23 shows the gap size of the lattice as a function of the interaction U. The dashed lines indicate the phase transitions and in the legend are the corresponding values.

The square lattice shows asymptotic behaviour for $t' \to 0$. The data can be fitted with the curve

$$[U_c(t')]^{-1} = \frac{c_1}{2} \ln(t')^2 + c_2 \ln(t') + c_3 \tag{3.65}$$

with the values $c_1 = 0.10$, $c_2 = -0.7$ and $c_3 = 0.24$ an $t' > 0$. Figure 3.24 includes the critical data points and the according fit.

For small t' the asymptotic function reduces, according to [17], to

$$[U_c(t')]^{-1} = \frac{1}{4\pi^2} \ln(t')^2 - 0.15 \ln(t'). \tag{3.66}$$

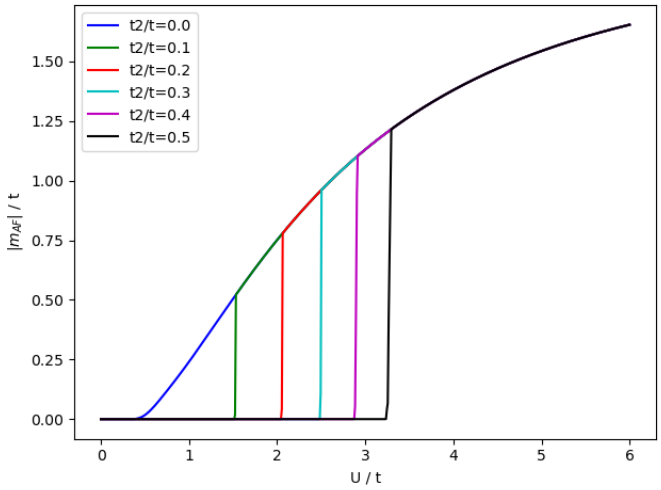

Figure 3.22: The antiferromagnetic parameter m_{AF} for the square lattice as a function of the on-site interaction U with the hopping parameters $0.0 \leq t'/t \leq 0.5$.

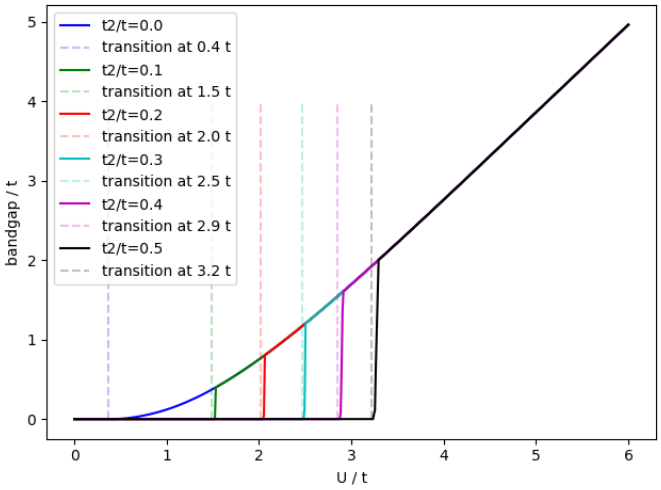

Figure 3.23: The gap size for the square lattice as a function of the on-site interaction U with the hopping parameters $0.0 \leq t'/t \leq 0.5$.

The comparison of asymptotic equations 3.65 and 3.66 shows that the additive constant is missing in the fitting function. The constant results from the finite critical interaction value U_c at perfect nesting conditions.

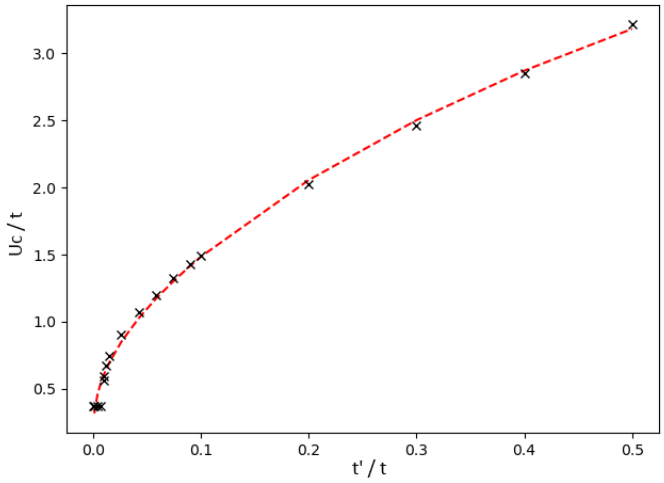

Figure 3.24: Critical value U_c as a function of the hopping t'/t.

Theoretically it should be zero, but because of the finite *epsilon*, there is a finite gap size and the critical U_c is greater than zero.

Honeycomb Lattice

With the inclusion of the next-nearest neighbour hopping the honeycomb lattice starts to change it's behaviour for a hopping constant of $t'_s/t \approx 0.33$. Figure 3.25 shows the dispersion relation of the lattice for a hopping constant of $t'/t = 0.33$. The red plane marks the chemical potential μ and the structure shows a change of the Fermi surface, where for $t'/t > 0.33$ additional Fermi points appear.

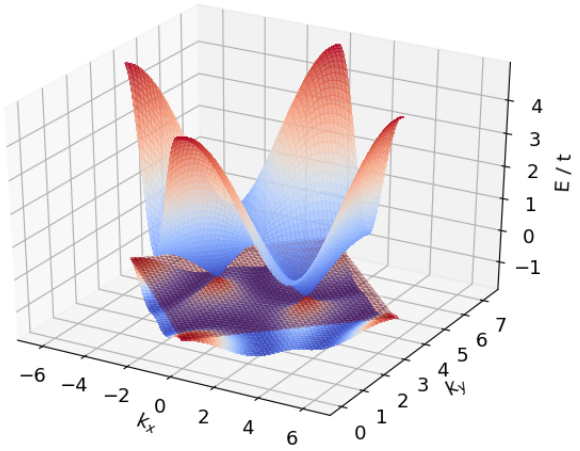

Figure 3.25: Dispersion relation for the hopping constant $t'/t = 0.33$ of the hexagonal lattice. The red plane marks the chemical potential to mark the change of the Fermi surface.

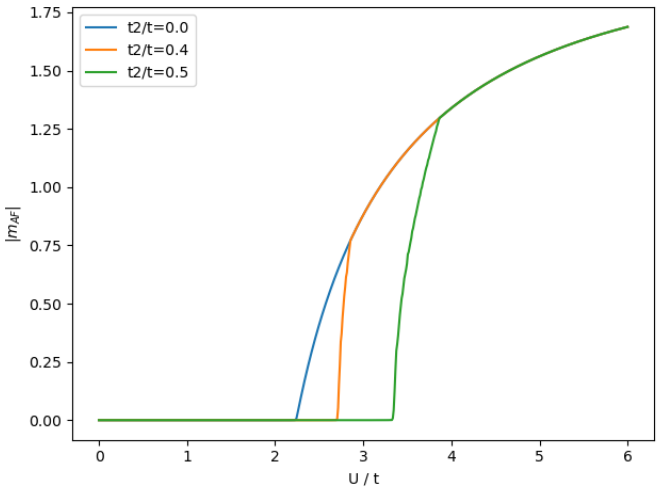

Figure 3.26: Antiferromagnetic parameter m_{AF} as a function of the on-site interaction U on the honeycomb lattice for three different hopping values $t'/t = [0.0, 0.4, 0.5]$.

Figure 3.26 shows the antiferromagnetic parameter m_{AF} as a function of the interaction parameter U. Figure 3.27 shows the gap size of the lattice as a

function of U. The gap size shows a continuous behaviour across the phase transition for any $t' > t'_s$.

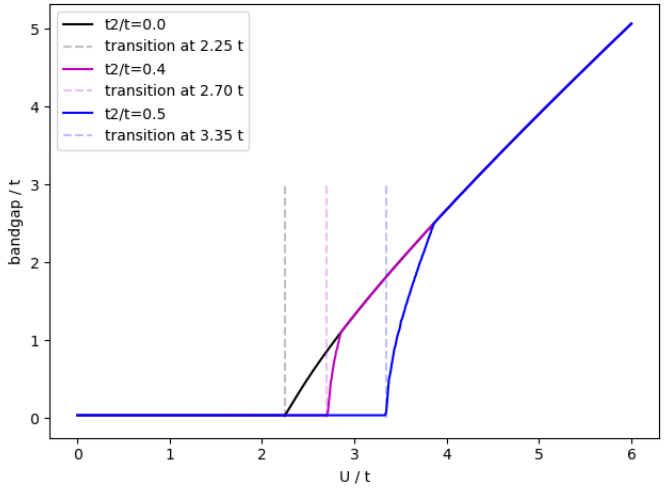

Figure 3.27: Gap size as a function of U for three different hopping values $t'/t = [0.0, 0.4, 0.5]$ on the honeycomb lattice. The dashed lines indicate the phase transitions.

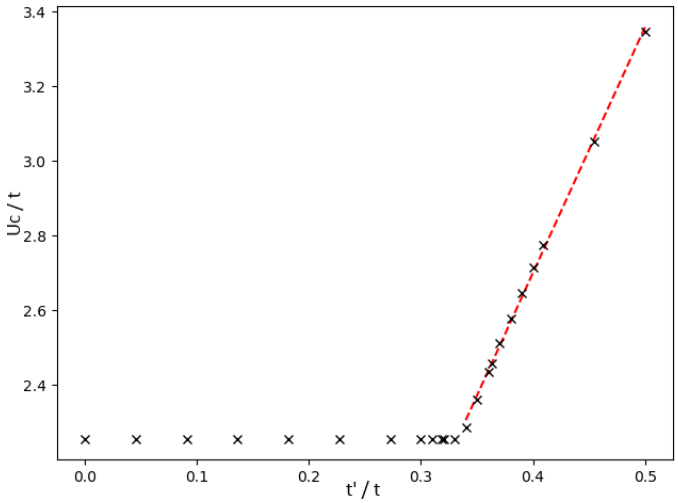

Figure 3.28: Critical value U_c as a function of the hopping t'/t.

For $t'/t > 0.33$, the behaviour of the critical transition value $U_c(t')$ as a

function of the second hopping t' is linear. The fitted function and the critical data points can be seen in figure 3.28. The fitted function has the form

$$U_c(t') = c_1 t' + c_2 \tag{3.67}$$

with the parameters $c_1 = 6.57$ and $c_2 = 0.07$.

Table 3.3 shows the critical transition values $U_c(t')$ to the according t'.

Table 3.3: Critical transition values $U_c(t')$ for the different next-nearest neighbour hopping constants t' for the hexagonal lattice.

t'/t	$U_c(t')/t$
0.0	2.3
0.4	2.7
0.5	3.4

4 Beyond Mean-Field

The one-dimensional extended Hubbard model is a useful model for quasi one-dimensional materials. This includes for example conducting polymers and organic charge-transfer [18]. There are three different phases at the

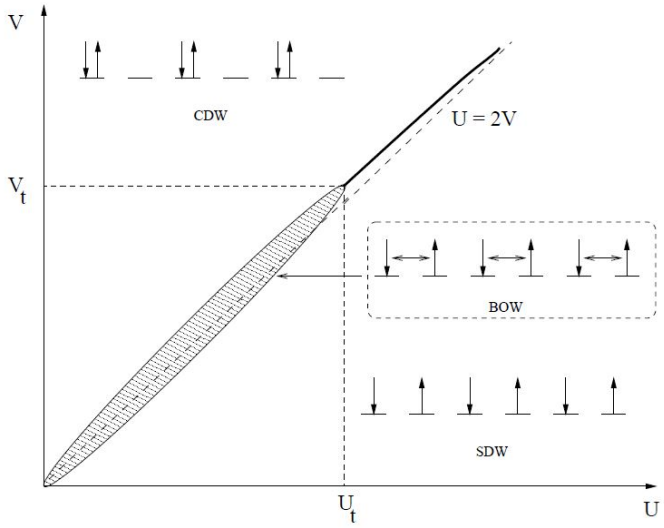

Figure 4.1: Phase diagram for the one-dimensional extended Hubbard model at half filling with three different phases (from [18]).

ground state phase diagram which can be seen in figure 4.1. It shows the already known CDW and SDW phases, and there is a bond-order-wave (BOW) phase in a narrow strip between the CDW and SDW phases. It appears for small to intermediate values for U and V. The characterization of the BOW phase is the alternating strengths of the expectation value for the kinetic energy operator at the bonds. The discrete symmetry is broken and it exhibits a true long-range order. The transition between CDW and SDW phases is separated in two different transitions. There is a continuous

transition from CDW to BOW and a Kosterlitz-Thouless spin-gap transition from BOW to SDW. The BOW phase vanishes at the multi-critical point and the remaining SDW and CDW phases have a direct and discontinuous transition.

The phase boundary between BOW and CDW phases involves a standard second order phase transition and can be well determined. The phase boundary between BOW and SDW phases involves a Kosterlitz-Thouless transition and is more difficult to locate. The transition is marked by the opening of a spin-gap in the electronic energy spectrum and the gap opens up exponentially slowly. The transition is only locatable for very big clusters and the Kosterlitz-Thouless transition is not studied in this work.

The presented method then performs a self-consistent mapping of the lattice problem onto an effective cluster model with $N_c > 1$ correlated sites. It reduces to the standard mean-field theory for $N_c = 1$. Because of the self-consistent procedure it is possible to study the symmetry broken phases, as explained in [19].

4.1 Beyond Mean-Field Hubbard Model

A system of interacting fermions on a lattice with a Hamiltonian H, consisting of a non-interacting term H_0 and an interaction term H_1, is given. Starting from the extended Hubbard Model, explained in chapter *'Models and Methods'* section 2.3 *'The extended Hubbard Model'*, the lattice is decoupled into small clusters with the size N_c. This gives the equation, as shown in [20],

$$H = \sum_{\mathbf{R}} H^{(c)}(\mathbf{R}) + \sum_{\mathbf{R},\mathbf{R'}} H^{(i)}(\mathbf{R},\mathbf{R'}), \tag{4.1}$$

where $\mathbf{R}$ denotes the individual clusters. The term $H^{(c)}(\mathbf{R})$ is the part that acts only inside a single cluster and the second term $H^{(i)}(\mathbf{R},\mathbf{R'})$ includes the coupling of different clusters, which is the only interaction between the clusters.

The two terms include

$$H^{(c)}(\mathbf{R}) = H_0^{(c)}(\mathbf{R}) + H_U^{(c)}(\mathbf{R}) + H_V^{(c)}(\mathbf{R}) \tag{4.2}$$

$$H^{(i)}(\mathbf{R}, \mathbf{R'}) = H_V^{(i)}(\mathbf{R}, \mathbf{R'}), \tag{4.3}$$

where the first line is the extended Hubbard Model. $H_0^{(c)}(\mathbf{R})$ is the single-particle hopping term, $H_U^{(c)}(\mathbf{R})$ and $H_V^{(c)}(\mathbf{R})$ are the Coulomb interaction parts on the cluster. The second line is the inter-cluster coupling, with $H_V^{(i)}(\mathbf{R}, \mathbf{R'})$, the interaction part between the cluster. There is no inter-cluster hopping term, $H_0^{(i)}(\mathbf{R}, \mathbf{R'})$, because the hopping is reduced to intra-cluster hopping.
The intra-cluster part equation 4.2 is solved exactly and there is a non-zero fluctuation δn in the cluster. The inter-cluster part equation 4.3 is solved via the mean-field approximation and the fluctuation with the neighbour cluster is $\delta n = 0$.

The inter-cluster two-particle interaction term is

$$H_V^{(i)}(\mathbf{R}, \mathbf{R'}) = V \sum_{[ij]} n_{\mathbf{R}i} n_{\mathbf{R'}j} \tag{4.4}$$

where the symbol [ij] stands for bonds that are connecting nearest neighbours in different clusters. In the case of nearest-neighbour interactions [ij] belongs to the cluster boundaries of two side-by-side clusters.

To reduce the coupling term from a two-particle interaction to a single-particle type a mean-field decoupling is applied. The inter-cluster term becomes

$$H_{V,MF}^{(i)}(\mathbf{R}, \mathbf{R'}) = V \sum_{[ij]} [n_{\mathbf{R}i} \langle n_{\mathbf{R'}j} \rangle + \langle n_{\mathbf{R}i} \rangle n_{\mathbf{R'}j} - \langle n_{\mathbf{R}i} \rangle \langle n_{\mathbf{R'}j} \rangle]. \tag{4.5}$$

$\langle n_{\mathbf{R}i} \rangle$ and $\langle n_{\mathbf{R'}j} \rangle$ are the mean-field parameters. Those are independent of $\mathbf{R}$ and $\mathbf{R'}$ and can be replaced by λ_i and λ_j. The calculation reduces to

$$\begin{aligned}\sum_{\mathbf{R},\mathbf{R'}} H^{(i)}_{V,MF}(\mathbf{R},\mathbf{R'}) &= V \sum_{\mathbf{R},\mathbf{R'}} \sum_{[ij]} [n_{\mathbf{R}i}\lambda_j + \lambda_i n_{\mathbf{R'}j} - \lambda_i\lambda_j] = \\ &= V \sum_{\mathbf{R}} \sum_{[ij]} [n_{\mathbf{R}i}\lambda_j + \lambda_i n_{\mathbf{R}j} - \lambda_i\lambda_j] = \sum_{\mathbf{R}} H^{(i)}_{V,MF}(\mathbf{R}).\end{aligned} \tag{4.6}$$

In equation 4.6 the two-site interactions couple at most two different clusters and the double sum reduces to a single sum.
A one-dimensional cluster of length N_c reduces to

$$H^{(i)}_{V,MF}(\mathbf{R}) = V \sum_{\mathbf{R}} [n_{\mathbf{R}1}\lambda_B + n_{\mathbf{R}N_c}\lambda_A + \lambda_A\lambda_B], \tag{4.7}$$

where the only decoupled bond connects sites 1 and N_c of different clusters, with λ_A at site 1 and λ_B at site N_c. The two values λ_A and λ_B are the expectation values of the electron densities on sites A and B. The two different mean-field parameters in an half-filled system can be written as $\lambda_A = 1 - \delta$ and $\lambda_B = 1 + \delta$ on sublattices A and B. The parameter δ has the range [0, 1]. With this solution there is only one mean-field parameter δ, which simplifies equation 4.7 to

$$H^{(i)}_{V,MF}(\mathbf{R}) = V \sum_{\mathbf{R}} [n_{\mathbf{R}1}(1+\delta) + n_{\mathbf{R}N_c}(1-\delta) - (1-\delta^2)]. \tag{4.8}$$

The problem is solved with and without periodic boundary conditions for the hopping part of the Hamiltonian. The periodic solution of the problem sees the cluster as a ring. The appropriate hopping terms are added within the cluster and the Hubbard-Model extends with the terms

$$H^{(c)}_P(\mathbf{R}) = -t(c^\dagger_{N_c+1,\sigma} c_{N_c,\sigma} + c.c.) = -t(c^\dagger_{1,\sigma} c_{N_c,\sigma} + c.c.), \tag{4.9}$$

where the fact that $c^\dagger_{N_c+1,\sigma} = c^\dagger_{1,\sigma}$ is used.

The total Hamiltonian for the beyond-mean-field problem is given by

$$H = -t\sum_{i,\sigma}(c^{\dagger}_{i,\sigma}c_{i+1,\sigma} + c.c.) + U\sum_{i} n_{i\uparrow}n_{i\downarrow} + V\sum_{i} n_i n_{i+1} - \mu\sum_{i} n_i + \\ +V\sum_{\mathbf{R}}[n_{\mathbf{R}1}(1+\delta) + n_{\mathbf{R}N_c}(1-\delta) - (1-\delta^2)] - t(c^{\dagger}_{1,\sigma}c_{N_c,\sigma} + c.c.). \tag{4.10}$$

The chemical potential is $\mu = \frac{U}{2} + 2V$ due to particle-hole symmetry at half filling and the coordination number in one-dimension is $z = 2$.

From the decoupling of the clusters there are additional parameters λ_A and λ_B which are the expectation values of the electron densities on sites A and B. The two parameters have to be determined in a proper way.

4.1.1 Self-consistent Calculation

It is possible to calculate the density parameters from a self-consistent calculation of the isolated cluster, as explained in chapter *'Mean-field approximation'* section 3.2 *'Self-consistent calculation'*. The expectation values are

$$\langle n_{i\sigma}\rangle = \langle\phi_0|\, n_{i\sigma}\,|\phi_0\rangle = \langle\phi_0|\, c^{\dagger}_{i\sigma}c_{i\sigma}\,|\phi_0\rangle\,, \tag{4.11}$$

where ϕ_0 is the ground state.

For a first-order phase transition, where there is a transition between an ordered and a disordered phase, this method works very well. The transition point is almost independent of the cluster size due to avoided level crossing. For a second-order phase transition this method will not give satisfying results. There is a discrepancy between the parameters calculated on the isolated cluster and the parameters that would give the optimal result in the thermodynamic limit.

4.1.2 Minimization of the free energy

The self-consistent calculation of mean-field parameters is equivalent to the minimization of the free energy F. The minimization of F can be used to find the expectation value of the density operators. The free energy of a system is given by

$$F = -\frac{1}{\beta} \ln Z, \tag{4.12}$$

where

$$Z = \mathrm{tr}\Big(e^{-\beta H(\mathbf{R},\delta)}\Big). \tag{4.13}$$

The derivative with respect to δ is

$$\frac{\partial F}{\partial \delta} = V \sum_{\mathbf{R}} \langle \sum_{[ij]} [n_{\mathbf{R}i} - n_{\mathbf{R}j} + 2\delta] \rangle, \tag{4.14}$$

where the index $\mathbf{R}$ can be suppressed, because all clusters are equivalent. The derivative of equation 4.14 is set zero, which leads to a self-consistency condition

$$\sum_{[ij]} [\langle n_i \rangle - \langle n_j \rangle + 2\delta] = 0. \tag{4.15}$$

In the case of one dimension this is

$$\langle n_N \rangle - \langle n_1 \rangle = 2\delta, \tag{4.16}$$

with only one decoupled bond [1N]. On site 1, it belongs to sublattice A and on site N to sublattice B. The free energy has a minimum with respect to the mean-field parameter δ by thermodynamic stability arguments. Figure 4.2 shows the free energy as a function of δ for a fixed value $U = 12t$ and variable values $12.5t \leq zV \leq 13.0t$. The plot shows first-order phase transitions, the minima have a level-crossing. A second-order phase transition would have a continuous decreasing of the minimum from a finite value to zero.

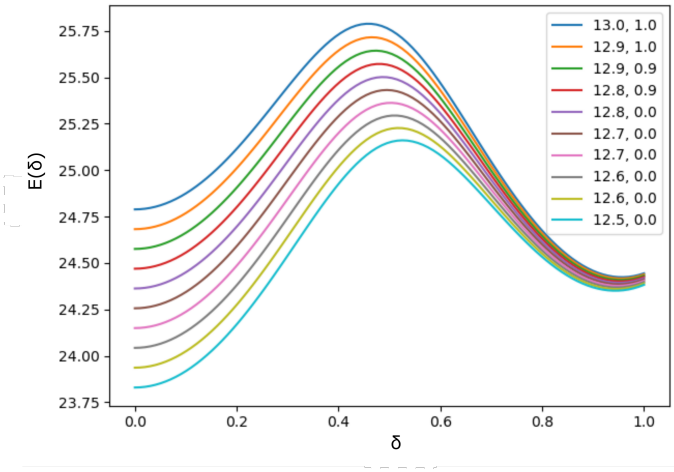

Figure 4.2: First order phase transitions for the interaction $U = 12t$ and different values for zV. The legend shows the value zV and the corresponding δ position of the minimum energy.

4.1.3 Calculation for $N_c = 2$

The easiest way to describe this method is by a cluster of size $N_c = 2$. This model consists of two sites labelled 1 and 2. The Hubbard model written explicitly looks like

$$H_{N_c=2} = -t(c_1^\dagger c_2 + c_2^\dagger c_1) + Un_{1\uparrow}n_{1\downarrow} + Un_{2\uparrow}n_{2\downarrow} + \\ + Vn_1n_2 + Vn_1\langle n_B\rangle + Vn_2\langle n_A\rangle, \tag{4.17}$$

where the next-neighbour hopping constant is zero $t'/t = 0$. Due to the half-filling condition we consider the number of electrons $N = 2$, with the number operator $N = \sum_{j\sigma} n_{j\sigma}$. The total spin quantum number is $S_z = 0$, with $S_z = \frac{1}{2}\sum_j (n_{j\uparrow} - n_{j\downarrow})$. Both quantum numbers commute with the Hamiltonian and are conserved quantities, as explained in [21]. The Hilbert space is four dimensional with four possible basis states $|\phi_J\rangle$ that are shown in table 4.1. The fourth column in the table, the binary representation, shows the states as direct product of the spin states.

Table 4.1: Four dimensional Hilbert space with $N = 2$ and $S_z = 0$ at half filling.

basis state	algebraic	picture	binary
$\|\phi_1\rangle$	$c^\dagger_{1\downarrow} c^\dagger_{1\uparrow} \|0\rangle$	$\uparrow\downarrow \circ$	$\|10\rangle_\downarrow \|10\rangle_\uparrow$
$\|\phi_2\rangle$	$c^\dagger_{1\downarrow} c^\dagger_{2\uparrow} \|0\rangle$	$\downarrow \uparrow$	$\|10\rangle_\downarrow \|01\rangle_\uparrow$
$\|\phi_3\rangle$	$c^\dagger_{2\downarrow} c^\dagger_{1\uparrow} \|0\rangle$	$\uparrow \downarrow$	$\|01\rangle_\downarrow \|10\rangle_\uparrow$
$\|\phi_4\rangle$	$c^\dagger_{2\downarrow} c^\dagger_{2\uparrow} \|0\rangle$	$\circ \uparrow\downarrow$	$\|01\rangle_\downarrow \|01\rangle_\uparrow$

The ground state in the Hilbert space is

$$|\phi_0\rangle = u'_1 |\phi_1\rangle + u'_2 |\phi_2\rangle + u'_3 |\phi_3\rangle + u'_4 |\phi_4\rangle . \tag{4.18}$$

The matrix representation of the Hubbard model, equation 4.17, in the Hilbert space can be written as

$$H = \begin{pmatrix} U + 2V\langle n_B\rangle & -t & -t & 0 \\ -t & 3V & 0 & -t \\ -t & 0 & 3V & -t \\ 0 & -t & -t & U + 2V\langle n_A\rangle \end{pmatrix} \tag{4.19}$$

The next step is the exact diagonalization (ED) of the matrix, where the eigenvalues and eigenstates are determined. The minimization of the free energy leads to new expectation values of the densities $\langle n_A\rangle$ and $\langle n_B\rangle$. A new matrix of the Hubbard model is set up and the calculation starts all over again. This procedure is repeated until convergence is achieved.

4.2 Phase transition and Phase diagram

The control parameter for the approximation is the size of the cluster. Clusters with two, four, six and eight sites are calculated. The next-nearest neighbour hopping constant is zero for the following solutions $t'/t = 0$.

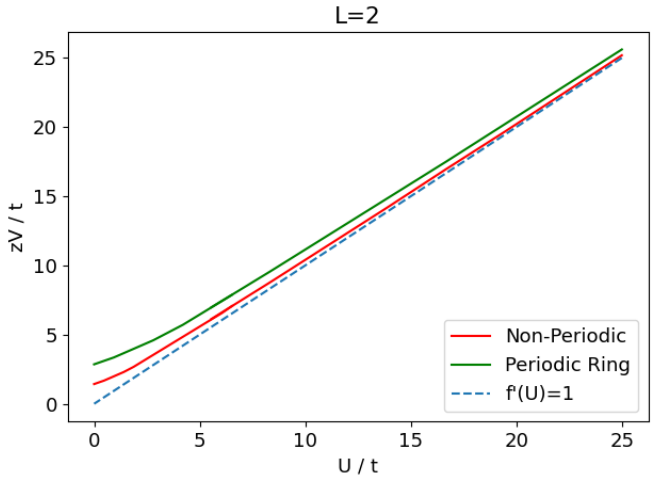

Figure 4.3: Phase transition in a one-dimensional lattice of the half filled extended Hubbard model with a cluster of the size $N_c = 2$.

Figure 4.3 shows the phase transition for cluster with size $N_c = 2$. The periodic ring mentioned in the legend defines the form of the cluster. If the condition is periodic, the form is a ring. If the condition is non-periodic, the cluster has the form of a bridge.

In the atomic limit, where $t = 0$, the phase boundary becomes a linear function $U = zV$. With finite t, there is energy gain of the order of t near the BOW-CDW instability, due to the competition between on-site and nearest neighbour Coulomb interaction, as explained in [10]. The ring usually overestimates the influence of the kinetic energy on the cluster and the open cluster, in form of a bridge, underestimates the kinetic energy. For the shown transition, the open cluster gives a function closer to the one of the atomic limit.

Figure 4.4 shows the phase transition in the one-dimensional lattice for a cluster of size $N_c = 4$.

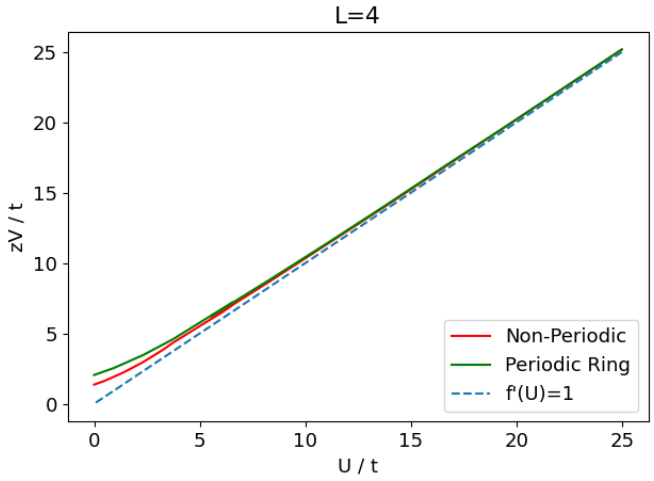

Figure 4.4: Phase transition in a one-dimensional lattice of the half filled extended Hubbard model with a cluster of the size $N_c = 4$.

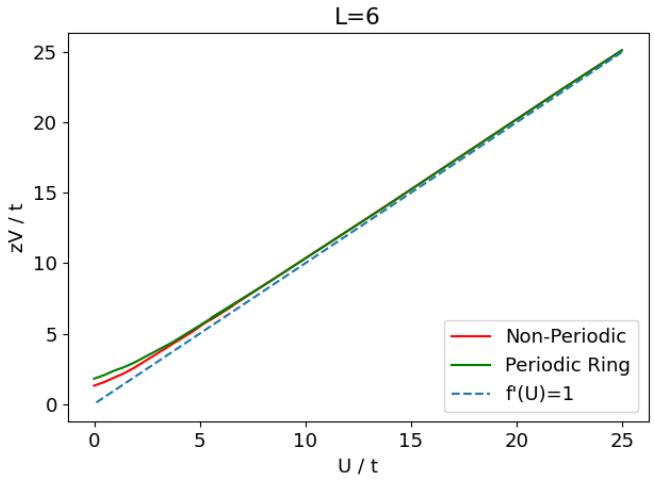

Figure 4.5: Phase transition in a one-dimensional lattice of the half filled extended Hubbard model with a cluster of the size $N_c = 6$.

Figure 4.5 shows the phase transition in the one-dimensional lattice for a cluster of size $N_c = 6$ and figure 4.6 shows the phase transition for a cluster of size $N_c = 8$.

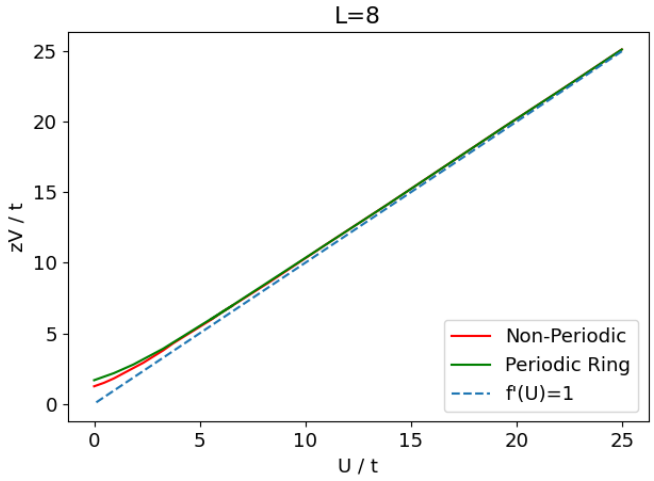

Figure 4.6: Phase transition in a one-dimensional lattice of the half filled extended Hubbard model with a cluster of the size $N_c = 8$.

Figure 4.7 shows the critical points zV_c for the on-site interaction $U = 5t$ at the different cluster sizes N_c. The cluster of size $N_c = 2$ is not taken into account for the scaling. The data is extrapolated by $1/L$. For $1/L \to 0$ the values become $zV_c^{(p)} = 5.21t$ for the periodic cluster and $zV_c^{(np)} = 5.38t$ for the non-periodic cluster. This values should have a scaling regime to the same point. The difference of the points can be explained by the small cluster sizes. In other literature [10] similar values can be found for a first order phase transition.

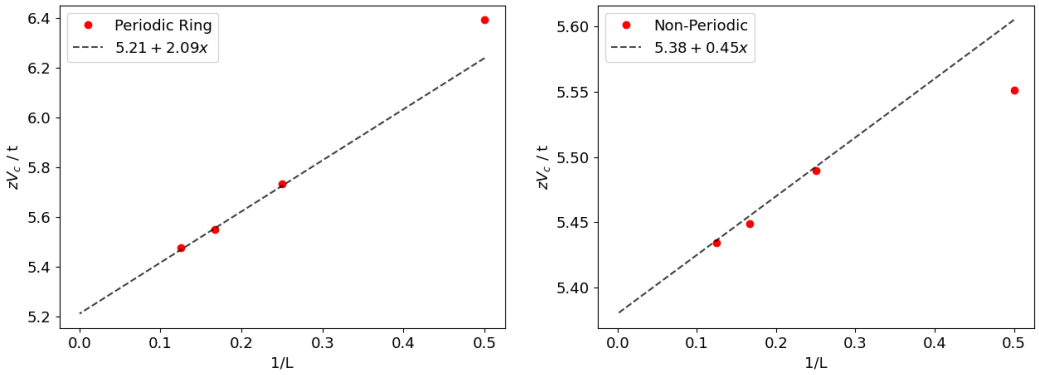

Figure 4.7: Periodic ring on the left and non-periodic open cluster on the right finite-size scaling at the interaction $U = 5t$. In the limit $1/L \to 0$ the critical values become $zV_c^{(p)} = 5.21t$ for periodic cluster and $zV_c^{(np)} = 5.38t$ for open cluster.

5 Conclusion

The one-dimensional and square lattices have strong tendency to the antiferromagnetic ordering in the case of perfect nesting without next-nearest neighbour hopping. For the phase transition of the spin-density wave, a critical value U_c of zero would be expected. For the one-dimensional and the square lattice, finite critical values were found. This is the consequence of a finite ϵ leading to a finite gap size.

The one-dimensional lattice has a critical value $U_c^{(1D)} = 0.58t$ ($V = 0$) and the square lattice has a critical value $U_c^{(SQ)} = 0.38t$ ($V = 0$). The SDW transition of the honeycomb lattice is at $U_c^{(HC)} = 2.25t$ ($V = 0$). The charge-density wave transition is at a critical value of zV_c. The critical values have a linear relationship $zV_c = \frac{U_c}{2}$. For the one-dimensional lattice the value is $zV_c^{(1D)} = 0.58t$ ($U = 0$). The square lattice has a CDW transition at $zV_c^{(SQ)} = 0.29t$ ($U = 0$) and the honeycomb lattice has the transition at $zV_c^{(SQ)} = 1.12t$ ($U = 0$). The honeycomb lattice does not have perfect nesting, because of the topology of the bands. The phase transitions are therefore very sharp.

To describe the effects of the loss of perfect nesting a next-nearest neighbour hopping t' was introduced. In the one-dimensional lattice the Fermi surface has a significant change at $t_s'^{(1D)}/t = 0.5$ and the perfect nesting gets destroyed. The values beyond $t_s'^{(1D)}$ has an asymptotic behaviour for $t' \to t_s'^{(1D)}$. The same is valid for the square lattice, with the value $t_s'^{(SQ)}/t = 0$. It has an asymptotic behaviour for $t' \to t_s'^{(SQ)}$. The honeycomb lattice has a change of the Fermi surface at the hopping constant $t_s'^{(HC)}/t = 0.33$. The t' values beyond $t_s'^{(HC)}$ have a linear behaviour for $t' \to t_s'^{(HC)}$.

The last method described in this work uses exact diagonalization combined with mean-field approximation to find a solution for the one-dimensional lattice. The cluster sizes are $N_c \in [2, 4, 6, 8]$. The critical interaction values depend on whether one takes open or periodic boundary conditions inside a cluster. Nevertheless, the results from open and periodic boundary conditions converge nicely towards each other for increasing cluster size. Also, a finite-size scaling has given extrapolated values for the critical interaction V_c that is in good accordance with literature.

Appendix A

Fourier Transformation

Hamiltonians have a locality in direct space, which means they connect sites in some defined distance. The locality in direct space is directly linked to a non-locality in Fourier space. This duality can be seen in the fact, that the kinetic energy of the Hamiltonian is intrinsic diagonal in Fourier space. The potential Energy of the Hamiltonian on the other hand is diagonal in direct space.

The non-diagonal Hamiltonian in real space can be diagonalized by the Fourier transform. The Fourier transform of the creation operator, described in equation 2.6, is

$$c^{\dagger}_{\mathbf{k}\sigma} = \frac{1}{\sqrt{N}} \sum_{i} e^{-i\mathbf{k}\mathbf{R_i}} c^{\dagger}_{i\sigma} \tag{5.1}$$

where N is the number of unit cells. This operator $c^{\dagger}_{\mathbf{k}\sigma}$ applied to the vacuum state creates a Bloch state. The Fourier transform in the annihilation operator, described in 2.7, is

$$c_{\mathbf{k}\sigma} = \frac{1}{\sqrt{N}} \sum_{\mathbf{k}} e^{i\mathbf{k}\mathbf{R_i}} c_{i\sigma}. \tag{5.2}$$

Bibliography

[1] Hubbard, J. (1963). *Electron correlations in narrow energy bands*. *Proceedings of the Royal Society of London. Series A, Mathematical and Physical Sciences*, 276(1365), 238-257.

[2] Peters, R. & Pruschke, T. (2008). *Half-filled Hubbard Model on a Bethe lattice with next-nearest neighbor hopping*. *Physical Review B*, 79(4). doi: 10.1103/PhysRevB.79.045108.

[3] Scalettar, R. T. (2016). *An Introduction to the Hubbard Hamiltonian*. In E. Pavarini, E. Koch, J. van den Brink, G. Sawatzky (eds). *Quantum Materials: Experiments and Theory* (5, 121-149). Jülich, Deutschland: Verlag des Forschungszentrum Jülich. ISSN 2192-8525.

[4] Szabo A. & Ostlund N. S. (1996). *Modern quantum chemistry: Introduction to Advanced Electronic Structure Theory*. Mineola, New York: Dover Publications. LCCN: lc96010775.

[5] P. Flude, P. Thalmeier, G. Zwicknagl (2006). *Strongly correlated electrons*. *Journal of Physics C: Solid State Physics*, 60. doi: 10.1016/s0081-1947(06)80003-2.

[6] Claveau, A., Arnaud, B., Di Matteo, S. (2014). *Mean-field solution of the Hubbard model: The magnetic phase diagram*. *European Journal of Physics*. 35(3), 035023. doi: 10.1088/0143-0807/35/3/035023.

[7] Hirsch, J. E. (1985). *Two-dimensional Hubbard model: Numerical simulation study*. *Physical review. B* 31(7), 4403-4419.

[8] Flude, P. (1995). *Electron correlations in molecules and solids* (3rd edition). Heidelberg, Berlin, Deutschland: Springer. doi: 10.1007/978-3-642-57809-0.

[9] Peters, R. & Pruschke, T. (2009). *Magnetic phase diagram of the Hubbard model with next-nearest-neighbour hopping*. *Physica B: Condensed Matter*, 404(19), 3249-3252. doi: 10.1016/j.physb.2009.07.083.

[10] Ejima S. & Nishimoto S. (2007). *Phase diagram of the one-dimensional half-filled extended Hubbard model*. *Physical Review Letters*, 99(21), 216403. doi: 10.1103/PhysRevLett.99.216403.

[11] Kashima, T. & Imada, M. (2001). *Magnetic and Metal–Insulator Transitions through Bandwidth Control in Two-Dimensional Hubbard Models with Nearest and Next-Nearest Neighbor Transfers*. *Journal of the Physical Society of Japan*, 70(10), 3052–3067. doi: 10.1143/jpsj.70.3052.

[12] Lin, H. Q. & Hirsch, J. E. (1987). *Two-dimensional Hubbard model with nearest- and next-nearest-neighbour hopping*. *Physical Review B*, 35(7), 3359-3368.

[13] Wallace, P. R. (1947). *The Band Theory of Graphite*, *Physical Review*, 71(9), 622-634. doi: 10.1103/PhysRev.71.622.

[14] Castro Neto, A. H., Guinea, F., Peres, N. M. R., Novoselov, S. S., Geim, A. K. (2009). *The electronic properties of graphene*. *Reviews of Modern Physics*, 81(1), 109-162. doi: 10.1103/revmodphys.81.109.

[15] Furukawa, N. (2001). *Antiferromagnetism of the Hubbard Model on a Layered Honeycomb Lattice - Is MgB_2 a Nearly-Antiferromagnetic Metal? -*. *Journal of the Physical Society of Japan*, 70, 1483-1486. doi: 10.1143/JPSJ.70.1483.

[16] Brouers, F. & Marconi, U. M. B. (1982). *On the antiferromagnetic phase in the Hubbard model*. *J. Phys. C: Solid State Phys.*, 15(26), L925-L928. doi: 10.1088/0022-3719/15/26/008.

[17] Hofstetter, W. & Vollhardt, D. (1998). *Frustration of antiferromagnetism in the $t - t'$-Hubbard model at weak coupling*. *Annalen der Physik*, 510(1), 48-55. doi: 10.1002/andp.19985100105.

[18] Sengupta, P., Sandvik, A. W., Campbell, D. K. (2002). *Bond-order-wave phase and quantum phase transitions in the one-dimensional extended Hubbard model*. *Physical Review B*, 65(15), 155113. doi: 10.1103/physrevb.65.155113.

[19] Dahnken, C., Aichhorn, M., Hanke, W., Arrigoni E., Potthoff M. (2004). *Variational cluster approach to spontaneous symmetry breaking: The itinerant antiferromagnet in two dimensions*. *Physical Review B*, 70(24), 245100. doi: 10.1103/physrevb.70.245110.

[20] Aichhorn, M., Evertz, H.G., von der Linden, W., Potthoff, M. (2004). *Charge ordering in extended Hubbard models: Variational cluster approach*. *Physical Review B*, 70(23), 235107. doi: 10.1103/PhysRevB.70.235107.

[21] Jafari, S. A. (2008). *Introduction to Hubbard model and exact diagonalization*. *Iranian Journal of Physics Research*, 8(2), 116-116.